*Published online 27 August 2022*

*Nucleic Acids Research, 2022, Vol. 50, No. 16* ***9319–9338***
*https://doi.org/10.1093/nar/gkac731*

# Topoisomerase IIA in adult NSCs regulates SVZ neurogenesis by transcriptional activation of Usp37

**Shangyao Qin[1,†], Yimin Yuan[1,†], Xiao Huang[1], Zijian Tan[1], Xin Hu[1], Hong Liu[1], Yingyan Pu[1], Yu-qiang Ding[2], Zhida Su[1,*] and Cheng He[1,*]**

[1]Institute of Neuroscience, Key Laboratory of Molecular Neurobiology of Ministry of Education and the Collaborative Innovation Center for Brain Science, Naval Medical University, Shanghai 200433, China and [2]Department of Laboratory Animal Science, and State Key Laboratory of Medical Neurobiology and MOE Frontiers Center for Brain Science, Institutes of Brain Science, Fudan University, Shanghai 200032, China

Received December 22, 2021; Revised July 31, 2022; Editorial Decision August 02, 2022; Accepted August 14, 2022

## ABSTRACT

**Topoisomerase IIA (TOP2a) has traditionally been known as an important nuclear enzyme that resolves entanglements and relieves torsional stress of DNA double strands. However, its function in genomic transcriptional regulation remains largely unknown, especially during adult neurogenesis. Here, we show that TOP2a is preferentially expressed in neurogenic niches in the brain of adult mice, such as the subventricular zone (SVZ). Conditional knockout of Top2a in adult neural stem cells (NSCs) of the SVZ significantly inhibits their self-renewal and proliferation, and ultimately reduces neurogenesis. To gain insight into the molecular mechanisms by which TOP2a regulates adult NSCs, we perform RNA-sequencing (RNA-Seq) plus chromatin immunoprecipitation sequencing (ChIP-Seq) and identify ubiquitin-specific protease 37 (Usp37) as a direct TOP2a target gene. Importantly, overexpression of Usp37 is sufficient to rescue the impaired self-renewal ability of adult NSCs caused by Top2a knockdown. Taken together, this proof-of-principle study illustrates a TOP2a/Usp37-mediated novel molecular mechanism in adult neurogenesis, which will significantly expand our understanding of the function of topoisomerase in the adult brain.**

## INTRODUCTION

Topoisomerases are enzymes that maintain the superstructure and integrity of chromosomes by modulating DNA topology (1). They disentangle topological problems arising from cellular processes such as DNA repair, transcription, replication and chromosome compaction, which is indispensable to cells (1). Despite decades of research, surprising findings of topoisomerases continue to emerge about their cellular function, regulation and utility as therapeutic targets (2–4).

In mammals, there are two types of topoisomerases: type I topoisomerases (TOP1 and TOP3) and type II topoisomerases (TOP2) (5). As the second most abundant chromatin protein in eukaryotes after histones, TOP2s have been traditionally known as duplex DNA 'strand-passage' enzymes that resolve entanglements and relieve torsional stress of DNA by the production of DNA double-stranded breaks (6,7). TOP2a and TOP2b are two isozymes of TOP2. They greatly resemble each other in the N-terminal ATPase and central core domains, but possess major differences in their C-terminus, which contains one or more homologous protein-interactive domains (8,9). Functionally, TOP2a is closely associated with the cell cycle and stem cell program validated in embryonic stem cells (ESCs), while TOP2b is mainly involved in cell fate commitment and differentiation (10,11). It is well documented that TOP2a is indispensable for the survival of cellular organisms and is a pivotal clinical target for anticancer and antimicrobial treatments (6,7). Genetic deletion of Top2a leads to embryonic lethality at the 4- or 8-cell stage, indicative of its irreplaceable roles in early embryogenesis in mice (12,13). Apart from its enzyme activity, the functions of TOP2a in genomic transcriptional regulation, especially during cellular specification and differentiation, are only beginning to be understood (10,14,15).

Adult neurogenesis appears to be very well conserved in mammals and plays a fundamental role in brain plasticity (16). In the adult brain, neurogenesis mainly occurs in two specialized neurogenic niches, the subventricular zone (SVZ) adjacent to the lateral ventricles (LVs) and the subgranular zone (SGZ) of the dentate gyrus (DG). Depending on the area of adult neurogenesis, new neurons are constantly generated from neural stem cells (NSCs) and inte-

*To whom correspondence should be addressed. Tel: +86 21 81871042; Fax: +86 21 65492132; Email: suzhida@smmu.edu.cn
Correspondence may also be addressed to Cheng He. Tel: +86 21 65515200; Fax: +86 21 65492132; Email: chenghe@smmu.edu.cn
†The authors wish it to be known that, in their opinion, the first two authors should be regarded as Joint First Authors

grated into existing neuronal circuits throughout life, while perturbation of adult neurogenesis leads to several human diseases, including cognitive impairment and neurodegenerative diseases (17–19). Therefore, unraveling how neurogenesis is regulated in adulthood is crucial for understanding the pathogenesis of several neurological disorders. Over the past decades, the interplay between extrinsic and intrinsic factors has been shown to regulate the activity of NSCs in adult neurogenesis (20–24), while the underlying mechanisms remain largely unknown. Based on the fact that TOP2a can direct and regulate the process of embryonic development (10,25), we here attempt to investigate the expression pattern of TOP2a in the central nervous system (CNS), especially in the adult brain, and to decipher its specific functions in adult neurogenesis.

In the present study, we show that TOP2a is preferentially expressed in the neurogenic niches in the adult brain and provide strong evidence for a novel transcriptional regulatory role of TOP2a in the context of adult neurogenesis, which is mediated by its direct target ubiquitin-specific protease 37 (Usp37).

## MATERIALS AND METHODS

### Animals

Adult male C57BL/6 mice were purchased from Shanghai Ling Chang Biotech Co., Ltd. and Gfap::CreERT2 mice were obtained from Jackson labs. Nestin::CreERT2 mice were a gift from Professor Ryoichiro Kageyama (Institute for Virus Research, Kyoto University). To conditionally delete Top2a in adult NSCs, we generated Top2a$^{Loxp/Loxp}$ mice, which were maintained on a C57BL/6 background. Because TOP2a contains three different kinds of protein domains, amino acids 28–264 exons 2–8), 254–416 (exons 7–11) and 430–1187 (exons 11–28), we selected exon 3 as the knockout target by which all the domains could be deleted according to the frameshift mutation. The CreERT2/loxP recombination system was induced by tamoxifen administration (Sigma, Cat#T5648; 10 mg/ml in 1:9 ethanol:corn oil), injected intraperitoneally daily for seven consecutive days (2 mg/injection).

Animals were housed in standard housing conditions on a normal 12 h light/dark cycle with food and water *ad libitum*. All experiments and animal care were performed in compliance with the National Institutes of Health Care and Use of Animals guidelines and were approved by the Animal Experimentation Ethics Committee of our university.

### Primary culture of SVZ-derived adult NSCs

Neurospheres formed by SVZ-derived adult NSCs were cultured according to a previously described protocol with minor modifications (26). In brief, 8-week-old C57BL/6 mice were sterilized with 75% alcohol after being sacrificed. Following the exposure of the cerebrum, we removed the meninges, olfactory bulb (OB) and cerebral cortex, and then tissues surrounding the LV were isolated. The tissues were digested by trypsin–EDTA (0.025%) and hyaluronidase (0.7 mg/ml) at 37°C for 25 min. The digestion was stopped by ovomucoid, and the tissues were dispersed into single-cell suspensions. Cells were seeded into 24-well plates (5 cells/μl) or T25 flasks (20–30 cells/μl) and cultured with NSC medium containing fibroblast growth factor 2 (FGF2) and epidermal growth factor (EGF) (both at 20 ng/ml, Invitrogen).

Cultured NSCs were treated with TOP2a short hairpin RNA (shRNA) or inhibitors, i.e. ICRF-193 (Sigma), VP-16 (Sigma) and PluriSIn#2 (also known as 1-phenylcarbamoyl-5-fluorouracil, Fuchun Biotech). The self-renewal ability of NSCs was assessed by quantitative analysis of the number and size of neurospheres. Briefly, the number of neurospheres formed per 10 000 cells isolated from the SVZ was quantified 10 days after the indicated treatments, and the diameter of these neurospheres was also measured by Image pro-Plus6.0.

### Lentivirus preparation

For RNA interference, lentiviral vectors encoding Top2a or Usp37 shRNA or a scramble shRNA were constructed as described previously (27), in which gene expression was driven by a human glial fibrillary acidic protein (GFAP) promoter. For Usp37 overexpression, cytomeglaovirus (CMV) enhancer-MCS-3FLAG-EF1-ZsGreen1-T2A-puromycin vector was used to create the CMV-Usp37 plasmid. Co-expressed green fluorescent protein (GFP) in the vectors was used to visualize virus-infected cells. The detailed sequences for Top2a or Usp37 shRNA and the primers for Usp37 are listed in Supplementary Table S2.

Lentivirus was produced in human embryo kidney (HEK) 293T cells by transient transfections with lentiviral vectors and the packaging plasmids (lentiviral vector: VSVG: $\Delta 8.9$ = 4:1.5:1.5). Then, lentivirus was collected, precipitated with polyethylene glycol 8000 and concentrated by centrifugation. The concentrated virus was stored at −80°C before use.

### Stereotactic virus injection

For direct *in vivo* infection of NSCs, 5 μl of lentivirus ($0.5-2 \times 10^9$ pfu/ml) solution was injected into the SVZ using a 5 μl Hamilton microliter syringe with a 33-gauge, 18° beveled needle. The injection coordinates were as follows: anterior/posterior, –0.1 mm; medial/lateral, +1.38 mm; and dorsal/ventral from the skull, −2.6 mm. After the needle was held for 1 min, the virus was slowly injected at a rate of 0.3 μl/min. At the end of injections, the needle was held at the injection site for another 3 min and then slowly withdrawn within 1 min. After the operation, animals were placed in an incubator at 25°C before they awoke. The recovery state and activity of the mice were observed on the second, third and seventh days.

### qRT–PCR and western blotting

The knockdown efficiency of shRNA for Top2a was measured by quantitative PCR (qPCR) and western blotting. For qPCR, NSCs infected by the shRNA lentivirus were collected for lysis. RNA extraction was performed with TRIzol reagent. RNA product was reverse transcribed into cDNA using the RevertAid First Strand cDNA Synthesis Kit (Thermo Scientific Fermentas) after removal of ge-

nomic DNA. The detailed procedure of PCR was as follows: 1 min at 95°C, followed by 40 cycles of 15 s at 95°C, 15 s at 60°C and 45 s at 72°C. Quantification of the expression of Top2a was normalized to that of glyceraldehyde phosphate dehdrogenase (Gapdh) or β-actin. Three independent experiments were performed with the $2^{-\Delta\Delta CT}$ method to evaluate the relative expression of mRNA. We used SYBR-GREEN as the reaction solution and LightCycler 96 (Roche) as the qPCR instrument in this process.

For western blotting analysis, total proteins were extracted from primary NSCs infected by specific lentivirus. The proteins were electrophoresed by 10% sodium dodecylsulfate (SDS)–polyacrylamide electrophoresis (PAGE) and then transferred onto nitrocellulose membranes. After being blocked with 5% non-fat milk, the membranes were incubated with specific primary antibodies against TOP2a (Abcam, Rabbit 1:1000), USP37 (Proteintech, rabbit, 1:500), CYCLIN-A (Santa Cruz, mouse, 1:100), CDT-1 (Abcam, rabbit, 1:1000), GAPDH (Proteintech, rabbit, 1:5000) or β-ACTIN (Proteintech, mouse, 1:5000). Immunoreactive bands were detected by secondary antibodies using chemiluminescence reagents (ECL, Amersham) or Alexa Fluor® secondary antibodies (Invitrogen) based on the manufacturer's instructions. The images of bands were obtained using the Odyssey infrared imaging system and processed by Image-Pro Plus 6.0 software. Quantitative analysis of western blots was performed by densitometry and the values were pooled and expressed relative to GAPDH or β-ACTIN.

### Immunocytochemical staining

Cultured NSCs were fixed with 4% paraformaldehyde (PFA) for 15 min at room temperature. After permeabilization with 0.6% Triton X–phosphate-buffered saline (PBS) for 15 min and blocking with 3% bovine serum albumin (BSA) in PBS for 1 h at room temperature, cells were incubated in the primary antibodies diluted in blocking solution, for 24–48 h at 4°C. The appropriate secondary antibodies conjugated to Alexa Fluor 488, 594 or 647 (Jackson ImmunoResearch, 1:200) were used for indirect fluorescence. Nuclei were counterstained with Hoechst 33342 (1:1000). Images of immunofluorescence staining were captured by a Nikon E660FN microscope or a Leica SP5 confocal laser scanning microscope. A detailed list of antibodies is available in Supplementary Table S3.

### Immunohistochemical staining

Animals were anesthetized with 2% pentobarbital (30 mg/kg body weight) and transcardially perfused with 4% PFA. Their brains were dissected, post-fixed in 4% PFA overnight and cryoprotected by placing in 20% sucrose for 3–4 days at 4°C. Both brain hemispheres were sectioned on a cryostat (Leica) set at 25 μm thickness and every fifth section was collected. After antigen retrieval in citrate buffer at 95°C for 20–25 min, the brain sections were permeabilized with 0.6% Triton X–PBS for 15 min and blocked with 3% BSA in PBS for 1 h at room temperature. Then, immunostaining was performed by incubating sections with the primary antibodies (Supplementary Table S3) diluted in the blocking solution at 4°C overnight, followed by secondary antibodies (Jackson ImmunoResearch, 1:200) for indirect fluorescence. Nuclei were counterstained with Hoechst 33342. The samples were imaged with a fluorescence microscope (Nikon E660FN) or a confocal laser scanning microscope (Leica SP5). Subsequent processing of the images was performed by Image-Pro Plus and Adobe Photoshop CS5.

### Cell proliferation assays

*In vitro*, 10 μM BrdU (5-bromo-2-deoxyuridine) was added to the cultured NSCs. For BrdU staining, the cultures were washed with 1× PBS and fixed with 4% PFA for 20 min. Then, 2 N hydrochloric acid was added to the cultures, followed by incubation for 30 min at 37°C. After hydrochloric acid was washed off, the cells were incubated with 0.1 mol/l sodium tetraborate for 5 min twice. Finally, BrdU incorporation was detected in the cells by immunostaining with BrdU antibody.

To label the proliferating cells *in vivo*, animals were intraperitoneally injected with BrdU at a dose of 100 mg $kg^{-1}$ body weight as previously described (28). For short-term labeling experiments, the mice received a BrdU injection three times at 2 h intervals and were sacrificed on the next day. For long-term label-retention studies, the mice were injected with BrdU once a day for seven consecutive days, and were killed 1 month after the last BrdU injection. BrdU immunostaining was performed as described above.

### Flow cytometry

For apoptosis analysis, cells from neurospheres were assessed using the MULTI SCIENCES Apoptosis Detection Kit with Annexin V–fluorescein isothiocyanate (FITC) and propidium iodide (PI; AP101). Staining was performed in accordance with the manufacturer's instructions. In brief, after treatment with dimethylsulfoxide (DMSO), PluriSIn#2, ICRF-193 or VP-16, the single-cell suspensions from neurospheres were washed with PBS, and the concentration was adjusted to $1 \times 10^6$ cells/ml with 500 μl of Annexin V binding solution. Then 5 μl of Annexin V–FITC and 10 μl of PI solution were added. After that, cell suspensions were incubated in the dark for 5 min at room temperature before flow cytometry (FACS) analysis with the Beckman Couter MoFlo XDP. Finally, Annexin $V^+/PI^-$ (early apoptosis) or Annexin $V^+/PI^+$ (late apoptosis) cells were counted and analyzed by FlowJo V10 software.

Cell cycle analysis was performed using a MULTI SCIENCES Cell Cycle Staining Kit (CCS012). The single-cell suspensions from neurospheres were mixed with DNA staining solution (PI and RNase A) and permeabilization solution for 30 min at room temperature. The cell cycle stage was identified by flow cytometry and further analyzed using ModFit LT 5.0 software.

### *In vivo* compound administration

TOP2a inhibitors were administered by intracerebroventricular (ICV) injection. PluriSln#2, ICRF-193 and VP-16 were initially diluted in 1 μl of DMSO plus 4 μl of artificial

CSF (119 mM NaCl, 26.2 mM $NaHCO_3$, 10 mM glucose, 1.25 mM $NaH_2PO_4$, 2.5 mM KCl and 1.3 mM MgCl) with final concentrations of 7.2, 0.18 and 0.18 mM, respectively. Following a skin incision of ∼1 cm over each mouse skull midline, a total volume of 5 μl of solution was injected with a Hamilton syringe driven by an infusion pump during 6 min into the left LV at the following coordinates: anteroposterior, −0.1 mm; mediolateral, 1 mm; and dorsoventral, −3 mm.

### Cell quantification *in vivo*

For quantification of cells *in vivo*, standard procedures of histological analysis were performed as previously described (29). A total of 3–5 animals were used for each condition. All quantification of immunostainings was based on analysis of at least five 25 μm coronal or sagittal sections per animal. In these serial sections, cells were calculated in the SVZ, rostral migratory stream (RMS) and OB. The results were expressed as number of cells per area. All data collection and analyses were performed by investigators blind to the treatment conditions.

### RNA-Seq

After treatment with PluriSIn#2 or DMSO for 3 days, cultured SVZ NSC-derived neurospheres were collected for RNA-sequencing (RNA-Seq) analysis. The RNA-Seq ($n = 3$ for each condition) was performed on an Illumina platform. Data produced from the sequencer were evaluated by the FastQC software (version 0.11.9, http://www.bioinformatics.babraham.ac.uk/projects/fastqc/), and the reads were aligned to the mouse genome (mm10) using the software STAR (Spliced Transcripts Alignment to a Reference, version 2.6.1a) (30). The alignment reads were counted with the software Htseq-count (version 0.12.4), and the count matrix was normalized using the DESeq2 R package (version 4.1.0). We then determined differentially expressed genes (DEGs) with a screening criterion of log2 fold change (|log2FC|) >1 and false discovery rate (FDR) <0.05 (31,32). The annotation of DEGs was also performed by the clusterProfiler R package, including Gene Ontology (GO) functional analysis and Kyoto Encyclopedia of Genes and Genomes (KEGG) metabolic pathway analysis (33).

### ChIP-Seq/ChIP-qPCR

Chromatin immunoprecipitation sequencing (ChIP-Seq; $n = 1$ for each condition) was also performed on the Illumina platform. The cultured NSCs were cross-linked in 1% formaldehyde for 15 min at room temperature, and the cross-linking was stopped with excess glycine (125 mM). Precipitations were scraped off and rinsed with 10 ml of 1× PBS, and the chromatin was then interrupted by an ultrasound system. Protease inhibitors, Pro G agarose and pre-cleared chromatin were mixed together for 1 h at 4°C. Fragmented chromatin was incubated with anti-TOP2a antibody or IgG (control) at 4°C overnight, and then centrifuged for 1 min at 3000 *g*. After Pro G agarose was removed, 5 M NaCl was used for de-cross-linking DNA and proteins. Finally, the chromatin in NSCs was purified and collected after RNase A was added and mixed thoroughly for 1 h at 37°C.

After DNA sequencing, the data with the fastq format were evaluated by the FastQC software. Reads were aligned to the mouse genome (mm10) using the BWA (version 0.7.17-r1188) software (34). The alignment ratio of each sample was >90%. The characteristic peaks of Top2a on chromatins were found by peak calling using the software MACS2 (version 2.1.4) (35), and a *q*-value <0.05 was set as the standard for screening characteristic peaks. Motif analysis was performed using the Homer (version 4.11) software (36). In addition, ChIP DNA was also used for ChIP-qPCR.

### Statistical analysis

All data were from at least three animals or experimental culture batches and were plotted as the mean ± SEM. Data were tested for a normal distribution, and statistical analysis was performed by Student's *t*-test, one-way analysis of variance (ANOVA) with Tukey's post-hoc test or Mann–Whitney U-test. The significance level for all tests was set as $P < 0.05$.

## RESULTS

### TOP2a is exclusively expressed in neurogenic niches in the adult brain

To systematically investigate the temporal and spatial expression pattern of TOP2a, we performed immunohistochemical analysis on the brain of embryonic (E13.5/E16.5), post-natal (P3/P7), adult (P60) and aged (>18 months) mice. Immunostaining of coronal sections showed that TOP2a was strongly and broadly expressed in the ventricular zone (VZ), the SVZ of the neocortex and the region called the lateral ganglionic eminence (LGE) at E13.5 (Figure 1A). In a time-dependent manner, the number of TOP2a-positive cells in the cortex decreased sharply with development (Figure 1A). In the adult brain, $TOP2a^+$ cells were exclusively distributed in the SVZ (Figure 1A). Of note, few $TOP2a^+$ cells were observed in the SVZ of aged mice (Figure 1A). In contrast, TOP2b, a homologous molecule of TOP2a, was ubiquitously expressed in the whole brain of adult mice (Supplementary Figure S1). In addition, we further examined the expression pattern of TOP2a in sagittal sections. Similarly, the $TOP2a^+$ cells were also mainly located in the SVZ system including the RMS (Supplementary Figure S2A, B). Since the SVZ can be divided into several subregions as previously reported (37), we then examined the accurate location of $TOP2a^+$ cells along the LV. As shown in Figure 1B, the SVZ was divided into five different subregions, i.e. the dorsal-roof wall of the LV (drSVZ), the dorsal-lateral wall of the LV (dlSVZ), the lateral wall of the LV (lSVZ), the ventral wall of the LV (vSVZ) and the middle wall of the LV (mSVZ). Quantitative analysis indicated that $TOP2a^+$ cells were mainly distributed in the dlSVZ (51.73 ± 12.74%) and vSVZ (24.59 ± 9.22%) (Figure 1C). The distribution of $TOP2a^+$ cells was examined in the RMS and OB (Figure 1D, E; Supplementary Figure S2A, C, D, F). We observed that the number of $TOP2a^+$ cells decreased with distance from the SVZ to the

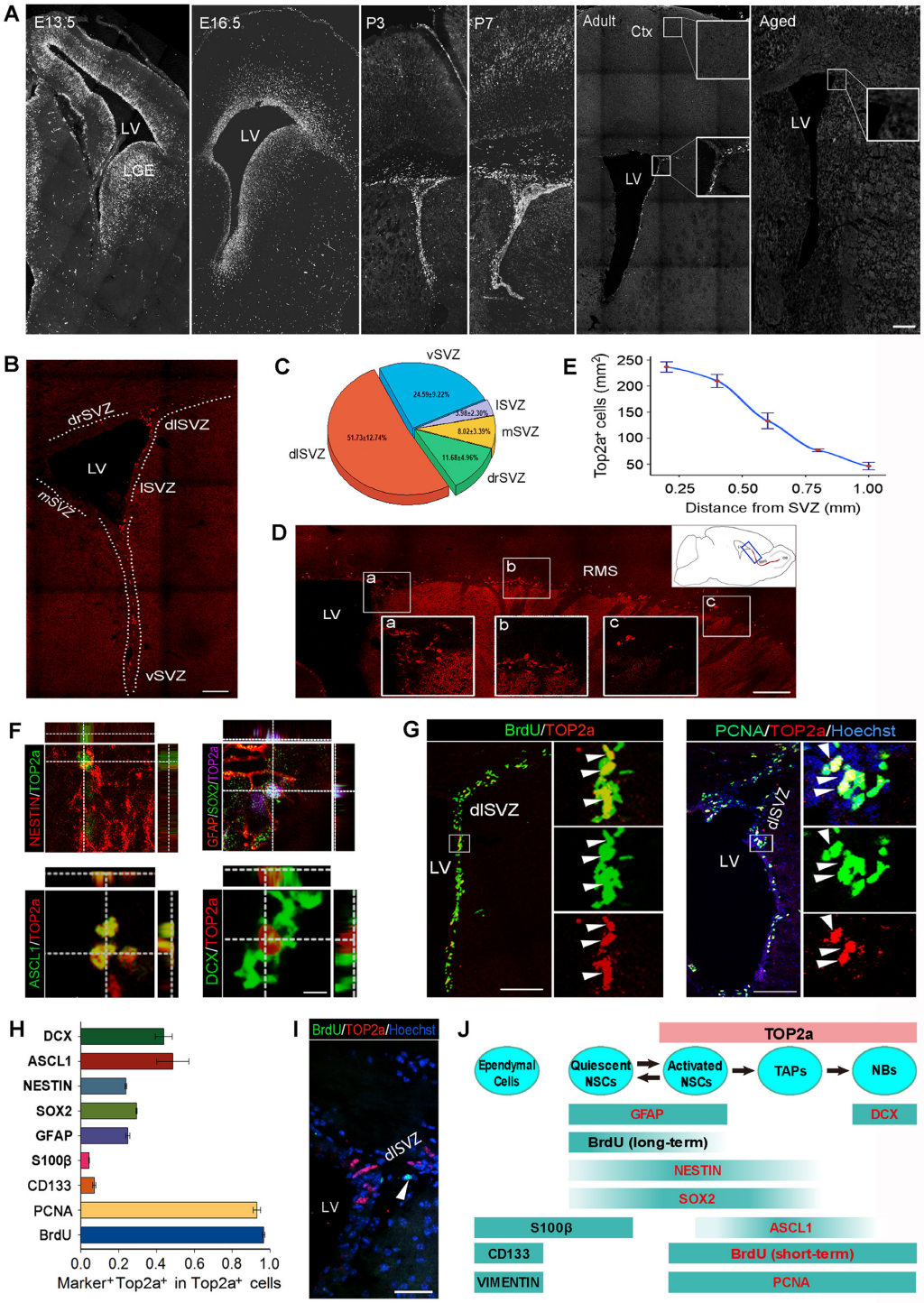


**Figure 1.** Expression pattern of TOP2a in developmenting and adult mouse brain. (**A**) The distribution of TOP2a differs in mouse brains at different developmental stages. Adult, 2–3 months of age; Aged, >18 months of age. (**B**) TOP2a$^+$ cells in the SVZ of adult brain. (**C**) Quantitative analysis of TOP2a$^+$ cells in (B) (mean ± SEM, $n = 3$ mice). (**D**) The expression of TOP2a in the RMS with different locations. The specific signal for Top2a expression is shown by the highly bright staining in the nuclear region (as indicated in the boxes). (**E**) Quantitative analysis of the number of TOP2a$^+$ cells in (D) (mean ± SEM, $n = 3$ mice). Briefly, the number of TOP2a$^+$ cells per mm$^2$ was quantified at different distances from the SVZ to the OB at the sagittal brain section. (**F**) Orthogonal views show that TOP2a is expressed in a flock of type B cells (NSCs), type C cells (TAPs) and type A cells (NBs) in the SVZ. (**G**) Short-term BrdU incorporation and PCNA proliferation assay for TOP2a$^+$ cells in the SVZ. (**H**) The percentage of different subpopulations of TOP2a$^+$ cells in the SVZ (mean ± SEM, $n = 3$ mice). (**I**) Long-term BrdU incorporation assay for TOP2a$^+$ cells in the SVZ. (**J**) Schematic diagram of TOP2a expression pattern in the SVZ of an adult mouse. LV, lateral ventricle; LGE, lateral ganglionic eminence; Ctx, cortex; drSVZ, dorsal-roof wall of the LV; dlSVZ, dorsal-lateral wall of the LV; lSVZ, lateral wall of the LV; vSVZ, ventral wall of the LV; mSVZ, middle wall of the LV; RMS, rostral migratory stream; NSCs, neural stem cells; TAPs, transit amplifying progenitors; NBs, neuroblasts. The scale bars represent 300 μm (A), 600 μm (B), 150 μm (D), 10 μm (F), 100 μm (G) and 40 μm (I).

OB (Figure 1E), and eventually disappeared in the OB (Supplementary Figure S2D). In addition to the SVZ–RMS–OB system, we also examined TOP2a expression in the DG of the hippocampus, another known neurogenic niche in the adult brain (38,39). As shown in Supplementary Figure S2E and F, there were only a few TOP2a$^+$ cells sparsely settled in the DG and co-labeled by the marker proliferating cell nuclear antigen (PCNA), consistent with the fact that the DG contains fewer NSCs than the SVZ in mice (26). Taken together, these findings indicate that TOP2a is specifically expressed in the neurogenic niches of adult brain, including the SVZ, RMS and DG, suggestive of a close relationship with adult neurogenesis.

In the SVZ, as shown in Supplementary Figure S3A, TOP2a$^+$ cells were co-labeled by TBR2, an SVZ marker that is specifically expressed in the amplifying progenitor cells. Quantitatively, there are 57.5 ± 15 TOP2a/TBR2 double-positive cells per square millimeter. Next, different NSC markers that label stem/progenitor cells at diverse stages of maturity were used for immunohistochemical analysis of the identity of TOP2a-expresssing cells in the SVZ. We found that TOP2a could be detected in NSCs (indicated by GFAP$^+$, NESTIN$^+$ or SOX2$^+$), transit amplifying progenitors (TAPs, indicated by ASCL1$^+$) and neuroblasts (NBs, indicated by DCX$^+$ (Doublecortin)) (Figure 1F, H; Supplementary Figure S3B–G), consistent with the single-cell RNA-Seq data from post-natal (40) and adult mouse brains (Supplementary Figure S4) (41). However, TOP2a was rarely detectable in ependymal cells (indicated by CD133$^+$, VIMENTIN$^+$ or S100β$^+$) (Figure 1H; Supplementary Figures S3G and S5). Furthermore, we conducted BrdU incorporation and PCNA immunostaining to test the proliferative state of TOP2a$^+$ cells. First, a short-term BrdU labeling experiment was performed to label the actively mitotic cells, in which animals received BrdU injection three times at 2 h intervals and were sacrificed on the next day. As shown in Figure 1G and H, the short-term BrdU labeling revealed that 96.68 ± 0.52% of TOP2a$^+$ cells in the SVZ were immunoreactive for BrdU. Immunohistochemistry for PCNA also indicated that 93.03 ± 1.70% of TOP2a$^+$ cells in the SVZ co-expressed PCNA (Figure 1G, H). We next performed a long-term BrdU label-retention experiment that could be used to identify slow-cycling quiescent stem cells in some adult tissues (28,42). In sharp contrast, long-term BrdU retention revealed that few TOP2a$^+$ cells were co-labeled by BrdU, hinting that TOP2a was not expressed in quiescent NSCs (Figure 1I). Collectively, these findings suggest that TOP2a is exclusively expressed in activated NSCs, TAPs and NBs (Figure 1H, J; Supplementary Figure S3F). These cells are in an actively proliferative state (Figure 1H, J; Supplementary Figure S3F), indicative of the fundamental molecular attribution of TOP2a in adult stem/progenitor cells in the SVZ.

### TOP2a is essential for the self-renewal of adult NSCs *in vitro*

Initially, NSCs were cultured from the SVZ tissues of adult mice (P60) (Figure 2A). The neurospheres derived from NSCs in the SVZ grew robustly *in vitro* and expressed the NSC markers, such as SOX2 and NESTIN (Supplementary Figure S6A). Notably, the vast majority of NSCs in the neurospheres incorporated BrdU, suggesting that they were actively proliferating cells (Supplementary Figure S6A). Single-neurosphere passaging revealed the extended self-renewal ability. There was no significant difference in sphere size between each passage, while the number of spheres increased with passages (Supplementary Figure S6B, C). In addition, the cultured NSCs were shown to possess the ability for multiple differentiation towards neurons, astrocytes and NG2-glia (Supplementary Figure S6D).

In order to determine the roles of TOP2a in adult NSCs, RNA interference was used to knock down Top2a. Three shRNAs (shRNA1–3) against Top2a were constructed in the lentiviral vectors in which the gene expression was driven by a human GFAP promoter (hGFAP) to specifically target NSCs, and the co-expressed GFP reporter was used to visualize the virus-infected cells (Figure 2A; Supplementary Figure S6E). Among these three shRNAs, qRT–PCR and western blotting showed that shRNA3 was able to significantly knock down TOP2a in NSCs (Supplementary Figure S7A, B), which was further confirmed by immunocytochemical analysis (Figure 2B,C). Therefore, shRNA3 (indicated by Top2a-shRNA) was used in the subsequent experiments. When Top2a was knocked down by shRNA, we found that both the number and the size of neurospheres formed by NSCs declined markedly (Figure 2D, E; Supplementary Figure S7C–E). Importantly, immunostaining revealed that Top2a knockdown in NSCs resulted in a marked decrease (∼67.2%) in the number of PCNA$^+$ cells, indicating that Top2a ablation also significantly compromised the proliferation level of NSCs (Figure 2F, G). Altogether, these findings suggest that TOP2a may be essential for the self-renewal of adult NSCs.

In addition, the effect of Top2a-shRNA on adult NSCs was further corroborated by experiments with chemical inhibitors, ICRF-193, VP-16 and PluriSIn#2. As shown in Figure 2H and I, neurosphere formation was significantly blocked by the treatment of NSCs with 500 nM ICRF-193 or VP-16. Of note, ICRF-193 and VP-16 may inhibit both Top2a and Top2b (9,10). To more specifically target Top2a, we also used another Top2a inhibitor—PluriSIn#2 (20 μM)—that has little effect on Top2b (43). Figure 2H and I revealed that both the number and size of neurospheres decreased dramatically after the treatment of NSCs with PluriSIn#2. Previous studies have indicated that inhibition of Top2a activity by ICRF-193 and VP-16 causes the formation of TOP2A/B–DNA complexes and DNA breakage, whereas PluriSIn#2 does not directly inhibit TOP2a enzymatic activity, but rather selectively represses its transcription (44,45). Although all these three chemical compounds were able to inhibit neurosphere formation, Figure 2J showed that only PluriSIn#2 resulted in a significant decrease of the Top2a expression level. Apoptosis detection using flow cytometry indicated that PluriSln#2 did not significantly affect the apoptosis of NSCs, whereas ICRF-193 and VP-16 resulted in significant apoptosis of NSCs (Supplementary Figure S8A, B). Of note, cell cycle analysis revealed that the treatment of NSCs with PluriSIn#2 induced them to arrest mainly in the $G_0/G_1$ phase, different from that in the $G_2/M$ phase by ICRF-193 and in the S phase by VP-16. (Supplementary Figure S8C, D). Collectively, these results are suggestive of a different mechanism

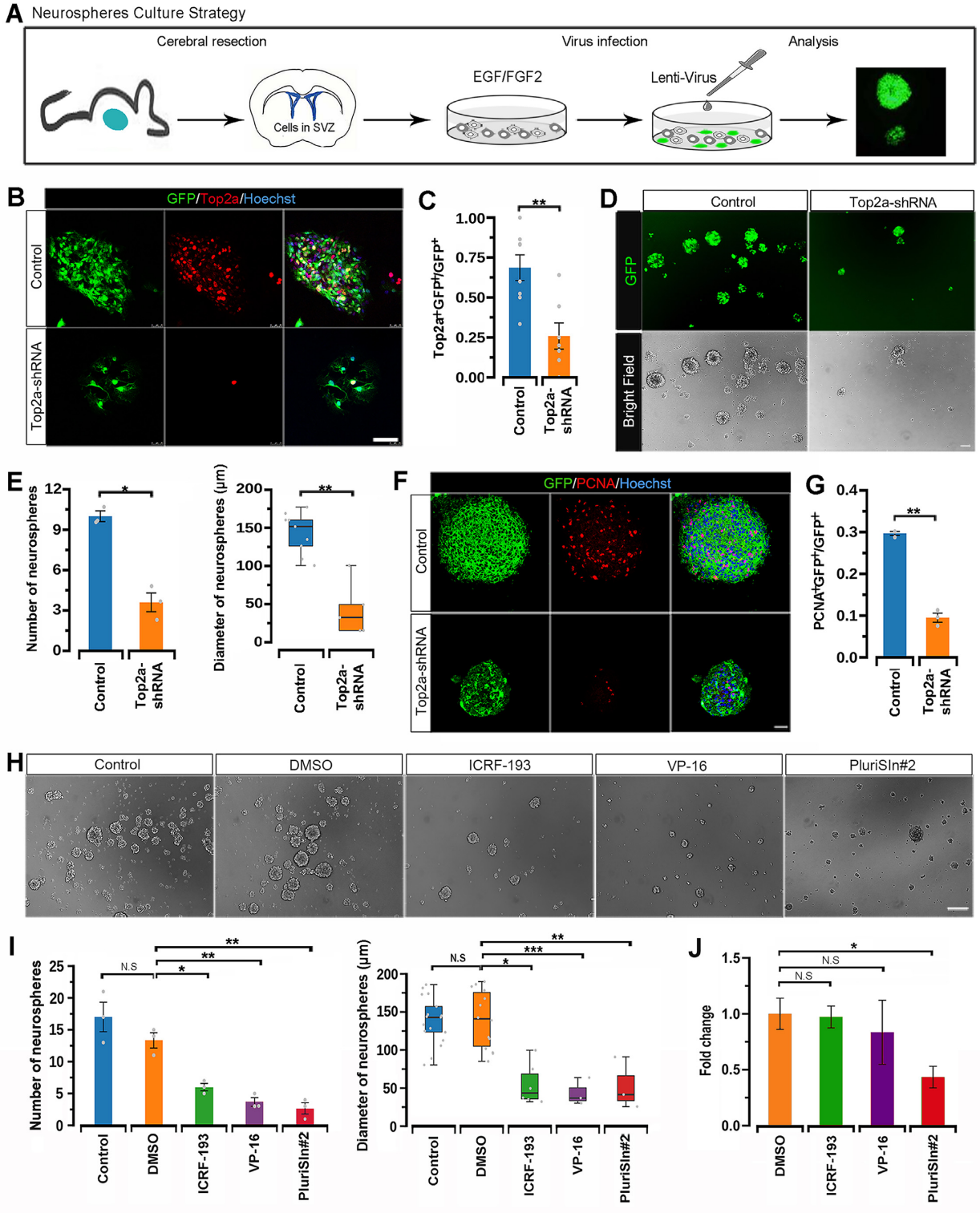


**Figure 2.** TOP2a is essential for the self-renewal of adult NSCs *in vitro*. (**A**) Schematic diagram showing the primary culture of adult NSCs and the administration of Top2a shRNA. (**B** and **C**) Expression of TOP2a in NSCs was significantly knocked down by shRNA. (**D** and **E**) The number and diameter of neurospheres were analyzed after Top2a-shRNA treatment. (**F** and **G**) After Top2a knockdown, the proliferation of NSCs in neurospheres was analyzed by immunostaining with PCNA. (**H** and **I**) The number and diameter of neurospheres were analyzed after treatment with DMSO or the Top2a inhibitors ICRF-193, VP-16 and PluriSIns#2. (**J**) qRT–PCR analysis of the Top2a expression level in NSCs from cultured neurospheres after treatment with DMSO or the Top2a inhibitors ICRF-193, VP-16 and PluriSIn#2. Data are plotted as the mean ± SEM. N.S., $P \geq 0.05$, *$P < 0.05$, **$P < 0.01$, ***$P < 0.001$ by Student's *t*-test (C, E and G) or one-way ANOVA with Tukey's post-hoc test (I and J). All experiments were performed at least three times independently. The scale bars represent 50 μm (B, D, F) and 150 μm (H).

of PluriSIn#2 from ICRF-193 and VP-16 and provide further evidence for the key role of TOP2a in the self-renewal of adult NSCs.

### TOP2a is essential for adult neurogenesis in the SVZ

The effect of TOP2a on cultured adult NSCs prompted us to probe its potential roles in adult neurogenesis *in vivo*. To this end, we conditionally deleted the Top2a gene in adult NSCs by Nestin::CreERT2-mediated combination. Animals heterozygous for Nestin::CreERT2 and homozygous (Nestin::CreERT2;Top2a$^{loxp/loxp}$) for the floxed Top2a allele were exposed to tamoxifen at 2 months of age (P60) (Figure 3A). The littermates that carry Top2a$^{loxp/loxp}$ but not CreERT2 activity were used as the control. Consistent with the qRT–PCR analysis (Figure 3B), immunohistochemical analysis showed that selective deletion of Top2a in the conditional knockout (CKO) mice (Nestin::Top2a$^{F/F}$) significantly reduced the number of TOP2a$^+$ cells in the SVZ to one-sixth of that seen in the control mice (Top2a$^{loxp/loxp}$), which received the same dose of tamoxifen at 2 months (Figure 3C), while no intervention of TOP2b expression was observed in the SVZ (Supplementary Figure S9). However, the conditional knockout of Top2a did not result in a significant change in the number of NESTIN$^+$ and SOX2$^+$ NSCs in the SVZ (Figure 3D, E). Because the NESTIN$^+$ or SOX2$^+$ NSCs include quiescent and activated NSCs, in which activated NSCs account for only a small fraction (46,47), we then examined the effects of TOP2a ablation on quiescent and activated NSCs, respectively. To determine whether Top2a knockout affects the activation of quiescent NSCs in the SVZ, we conducted the long-term BrdU label-retention experiments before the induction by tamoxifen (Figure 3F). Immunohistochemical analysis of the BrdU label-retention cells (BrdU-LRCs) showed that the number of quiescent NSCs (indicated by BrdU$^+$/NESTIN$^+$) in the SVZ was maintained at an equivalent level between Nestin::Top2a$^{F/F}$ and control mice, indicative of no effect of TOP2a on the activation of quiescent NSCs (Figure 3G). In order to examine whether Top2a deletion influences activated NSCs, immunostaining with PCNA and NSC markers was performed in the SVZ. It is interesting to note that the number of Ki67$^+$/NESTIN$^+$ or Ki67$^+$/SOX2$^+$ activated NSCs significantly decreased in Nestin::Top2a$^{F/F}$ compared with that in control mice (Figure 3H, I). These data suggest that Top2a knockout results in a significant loss of activated but not quiescent adult NSCs.

Next, we investigated whether selective deletion of Top2a in adult NSCs affects the generation of their progeny cells, including TAPs and NBs. When hGFAP promoter-driven Top2a-shRNA virus was injected into the SVZ, we found that the number of TOP2a$^+$ cells, as well as TOP2a$^+$/GFP$^+$ cells, was markedly diminished (Figure 4A, C). Remarkably, the number of PCNA$^+$ or PCNA$^+$/GFP$^+$ cells in the SVZ was also reduced considerably, illustrating that TOP2a knockdown by shRNA resulted in a significant decrease in the proliferation activity in the SVZ (Figure 4B, D). Using the Nestin::Top2a$^{F/F}$ transgenic mice, similarly, we observed that the number of PCNA$^+$ or TOP2a$^+$/PCNA$^+$ cells in the SVZ was dramatically decreased after conditional knockout of Top2a in NSCs (Figure 4E, F). Importantly, selective deletion of Top2a in NSCs also led to an obvious reduction in the number of ASCL1$^+$ TAPs and DCX$^+$ NBs (Figure 4G–J). Compared with the control mice, they were reduced by 60.9% and 54.4% in the SVZ of Nestin::Top2a$^{F/F}$ mice, respectively (Figure 4G–J). In addition to the Nestin::Top2a$^{F/F}$ mice, we also generated other transgenic mice, Gfap::Top2a$^{F/F}$, by Gfap::CreERT2-mediated combination to conditionally delete the Top2a gene in GFAP-positive NSCs in the SVZ (Supplementary Figure S10A). After the tamoxifen induction, Top2a was effectively knocked out in the SVZ of Gfap::Top2a$^{F/F}$ mice (Supplementary Figure S10B–D). In accordance with the results in Nestin::Top2a$^{F/F}$ mice, selective knockout of the Top2a gene in NSCs of Gfap::Top2a$^{F/F}$ mice did not influence the number of GFAP-positive NSCs in the SVZ (Supplementary Figure S10E, F), whereas it resulted in a significant decrease in the number of proliferating cells and NSC progeny cells (ASCl1$^+$ TAPs and DCX$^+$ NBs) in the SVZ (Supplementary Figure S10G–I). Interestingly, a similar phenotype was also observed in the adult mice treated with chemical inhibitors PluriSln#2, ICRF-193 and VP-16 (Supplementary Figure S11A–C). Of note, PluriSln#2 did not significantly affect the apoptosis of the SVZ NSCs, whereas ICRF-193 and VP-16 resulted in significant apoptosis (Supplementary Figure S11D, E), suggestive of different mechanisms mediated by these three inhibitors. Taken together, these findings indicate that TOP2a is required for the generation of NSC progeny cells to maintain adult neurogenesis in the SVZ.

### TOP2a is essential for the maintenance of adult neurogenesis in the OB

DCX$^+$ NBs, the progeny cells of NSCs in the SVZ, can migrate tangentially through the SVZ to the distal OB and then migrate radically from the granule cell layer (GCL) to the glomerular layer (GL) of the OB, where they ultimately become interneurons and integrate into the neuronal circuitry (48,49). Therefore, we further investigated whether conditional knockout of Top2a in adult NSCs affects the neurogenesis in the OB. First, immunohistochemical analysis was performed with antibodies against calretinin (CR), calbindin (CB), parvalbumin (PV) and tyrosine hydroxylase (TH) to label different types of neurons (Supplementary Figure S12A–C). As shown in Supplementary Figure S12D, there was no significant difference in the total number of CR$^+$, CB$^+$, PV$^+$ or TH$^+$ interneurons in the OB between Nestin::Top2a$^{F/F}$ mice and the control mice. As newborn interneurons only account for a small proportion of the total number of neurons in the OB, we then examined whether selective deletion of Top2a resulted in a decrease in the number of newborn interneurons. Nestin::Top2a$^{F/F}$ and control mice were treated with tamoxifen for seven consecutive days, and BrdU was injected intraperitoneally to label newly generated neurons in the OB after a 7 day clearing process (Figure 5A). Three weeks later, immunohistochemistry showed that BrdU-traced newborn cells in the GCL and GL of the OB decreased by 60.9% and 73.6%, respectively, as a result of Top2a knockout (Figure 5B, C). Importantly, BrdU and DCX double-staining showed that Top2a deletion resulted in a significant decrease of new-

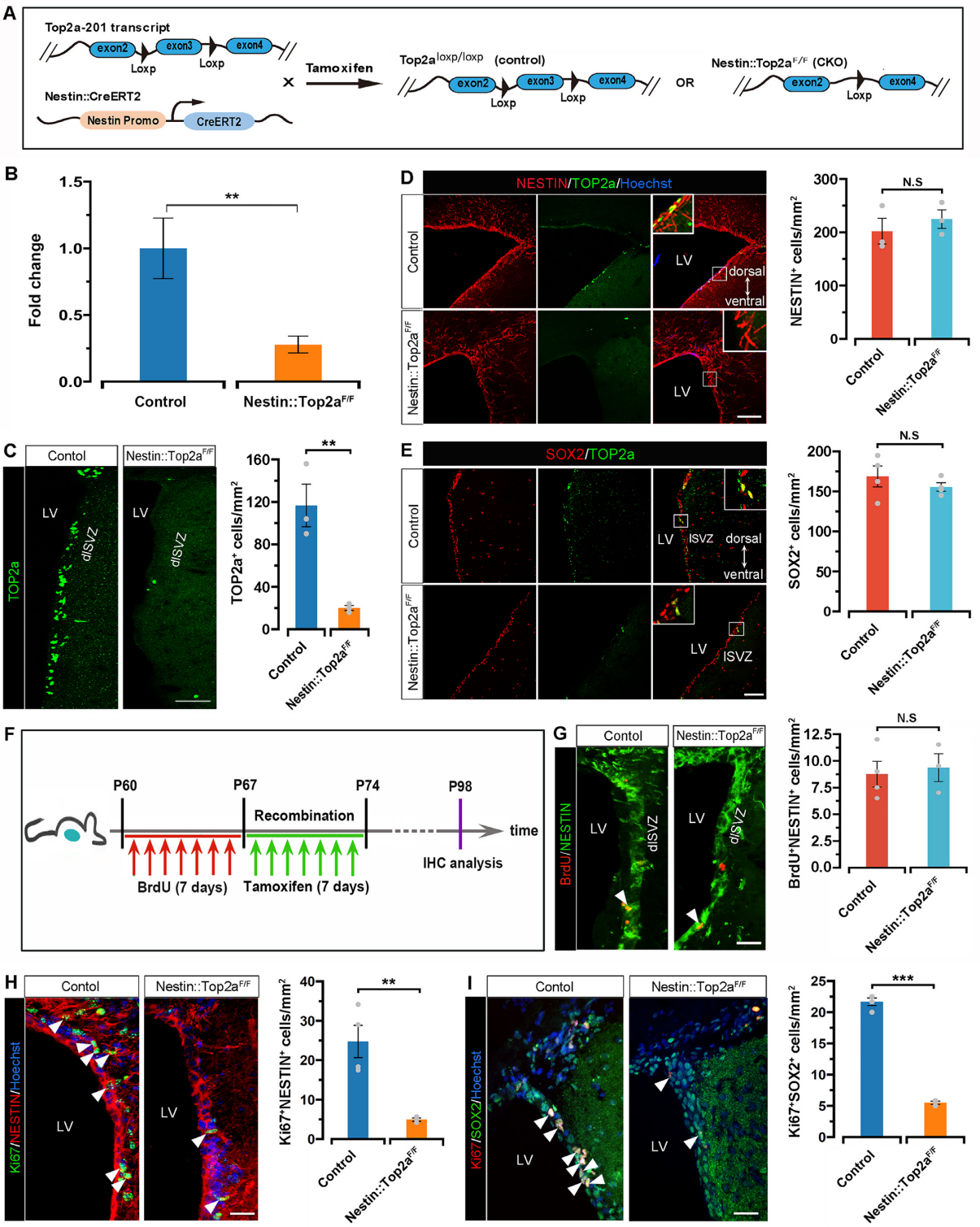


**Figure 3.** Conditional knockout of the Top2a gene in the Nestin::Top2a$^{F/F}$ mouse influences the number of activated but not quiescent adult NSCs in the SVZ. (**A**) Experimental scheme illustrating the generation of the Nestin::Top2a$^{F/F}$ mouse for conditional knockout of Top2a. (**B**) qRT–PCR of SVZ-derived cells showed the relative expression of Top2a between the control and Nestin::Top2a$^{F/F}$ transgene mice (mean ± SEM, $n = 3$ mice). (**C**) TOP2a expression decreased dramatically in the SVZ of the Nestin::Top2a$^{F/F}$ mouse (mean ± SEM, $n = 3$ mice). (**D** and **E**) The numbert of NESTIN$^+$ (D) and SOX2$^+$ (E) cells in the SVZ remained steady after conditional knockout of TOP2a (mean ± SEM, $n = 3$–4 mice). (**F**) Schematic diagram of the long-term BrdU label-retention experiments. (**G**) Quantification of the number of BrdU$^+$/NESTIN$^+$ cells in the SVZ of control and Nestin::Top2a$^{F/F}$ mice (mean ± SEM, $n = 3$–4 mice). (**H** and **I**) Quantitative analysis of Ki67$^+$/NESTIN$^+$ and Ki67$^+$/SOX2$^+$ cells in the SVZ of control and Nestin::Top2a$^{F/F}$ mice (mean ± SEM, $n = 3$ mice). N.S., $P \geq 0.05$, $^{**}P < 0.01$, $^{***}P < 0.001$ by Student's $t$-test. LV, lateral ventricle; dlSVZ, dorsal-lateral wall of LV; lSVZ, lateral wall of LV. The scale bars represent 100 μm (C, E), 75 μm (D) and 20 μm (G, H, I).

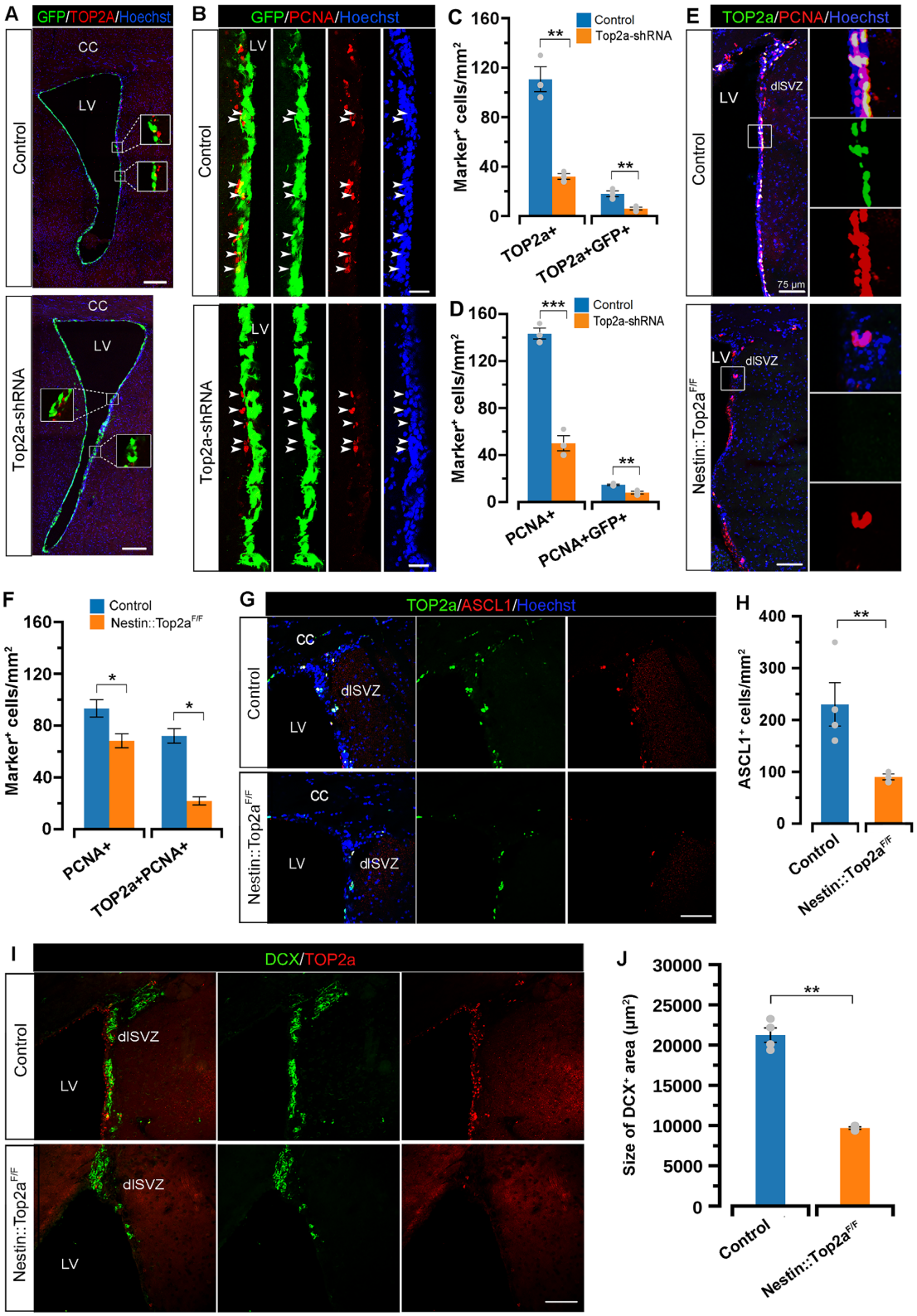


**Figure 4.** Conditional knockout of the Top2a gene in the Nestin::Top2a$^{F/F}$ mouse decreases the number of NSC progeny cells in the SVZ. (**A**–**D**) After injection of hGFAP-driven Top2a-shRNA virus into the SVZ, the expression of TOP2a and cell proliferation were quantitatively analyzed (mean ± SEM, $n = 3$ mice). The virus and proliferating cells were labeled by GFP and PCNA, respectively. (**E** and **F**) The cell proliferation in the SVZ was quantitatively analyzed by immunostaining with PCNA and TOP2a in the brain of Nestin::Top2a$^{F/F}$ and control mice (mean ± SEM, $n = 3$–4 mice). (**G**–**J**) Immunohistochemical analysis of ASCL1$^+$ TAPs and DCX$^+$ NBs in the SVZ of Nestin::Top2a$^{F/F}$ and control mice. Quantification showing that the number of ASCL1$^+$ cells (TAPs) and the size of the DCX$^+$ (NBs) area are markedly decreased after conditional knockout of Top2a (mean ± SEM, $n = 3$–4 mice). *$P$ <0.05, **$P$ <0.01, ***$P$ <0.01 by Student's $t$-test. CC, corpus callosum; LV, lateral ventricle; dlSVZ, dorsal-lateral wall of the LV. The scale bars represent 200 μm (A), 30 μm (B) and 75 μm (E, G, I).

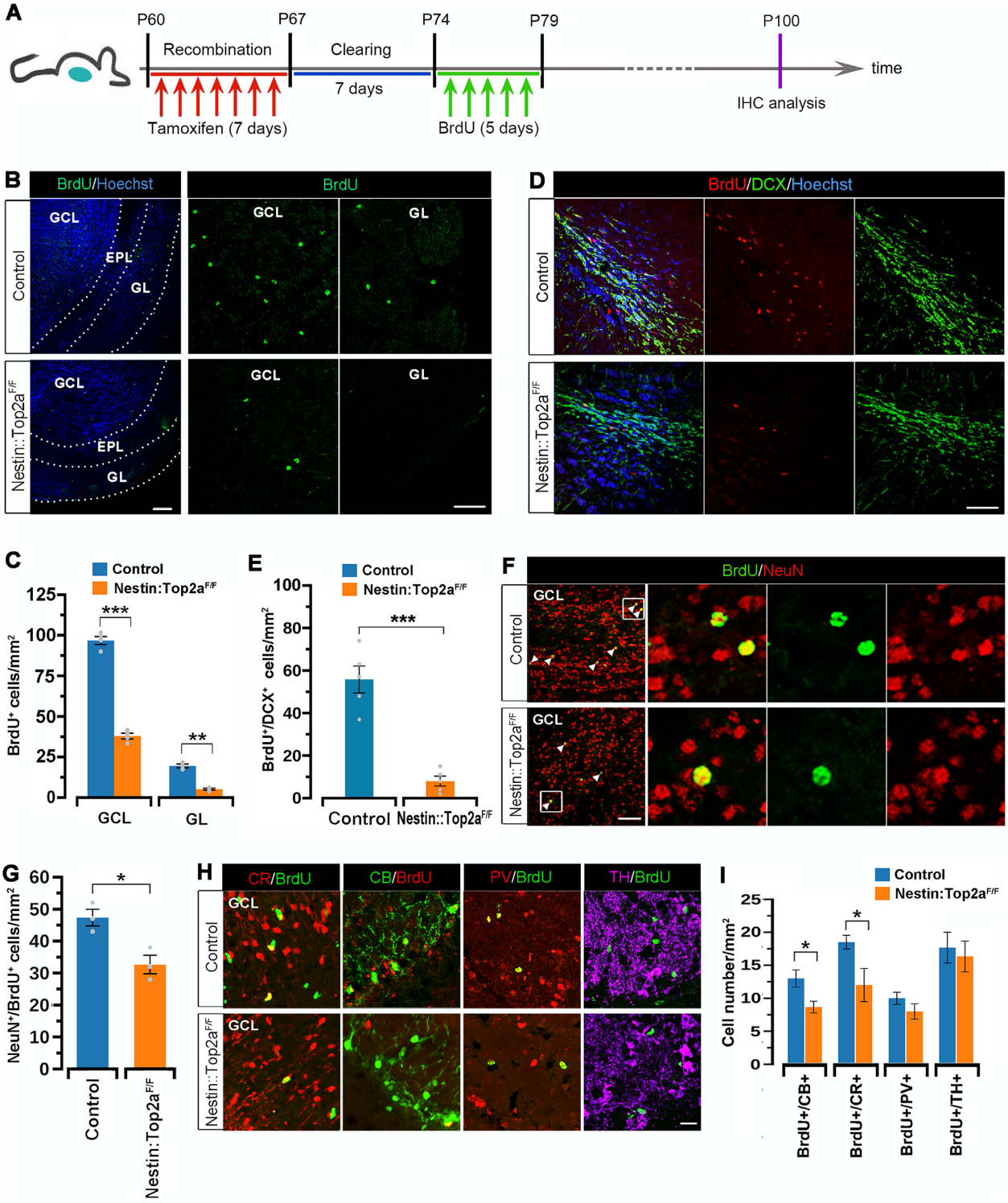


**Figure 5.** Conditional knockout of the Top2a gene in the Nestin::Top2a$^{F/F}$ mouse impedes adult neurogenesis in the OB. (**A**) Experimental scheme for tracing the SVZ-derived newborn neurons in the OB by BrdU labeling. (**B** and **C**) Immunohistochemical analysis of BrdU-traced newborn cells after Top2a deletion. BrdU$^+$ cells were quantified in the GCL and GL of the OB, respectively (mean ± SEM, $n$ = 3–4 mice in each group). (**D** and **E**) Immunohistochemical analysis of BrdU and DCX double-positive neurons after Top2a deletion. BrdU$^+$/DCX$^+$ cells were quantified in the GCL of the OB (mean ± SEM, $n$ = 3–4 mice in each group). (**F** and **G**) Quantitative analysis of BrdU and NeuN double-positive neurons in Nestin::Top2a$^{F/F}$ and control mice (mean ± SEM, $n$ = 3 mice). (**H** and **I**) Quantitative analysis of different types of interneurons in the OB (mean ± SEM, $n$ = 3–4 mice). *$P$ <0.05, **$P$ <0.01, ***$P$ <0.01 by Student's $t$-test. GCL, granule cell layer; EPL, external plexiform layer; GL, granular layer. CR, calretinin; CB, calbindin; PV, parvalbumin; TH, tyrosine hydroxylase. The scale bars represent 100 μm (B, D), 50 μm (F) and 20 μm (H).

born $BrdU^+/DCX^+$ immature neurons in the OB (Figure 5D, E). We further tested the cell identity of $BrdU^+$ cells by immunostaining for NeuN, a classical marker of mature neurons. Figure 5F showed that a majority of the $BrdU^+$ cells in the OB co-expressed NeuN, indicating that they were newborn neurons. Of note, conditional knockout of Top2a in NSCs led to a significant decrease in the number of $NeuN^+/BrdU^+$ cells (newly generated neurons) (Figure 5G). By immunohistochemical analysis with specific markers for different subtypes of interneurons, intriguingly, we found that BrdU-traced $CR^+$ and $CB^+$ newborn interneurons in the OB decreased by 35.1% and 33.3% in Nestin::$Top2a^{F/F}$ mice, respectively (Figure 5H, I). However, the number of BrdU-traced $PV^+$ and $TH^+$ newborn interneurons remained steady (Figure 5H, I). Together, these results suggest that selective deletion of Top2a in NSCs impedes the adult neurogenesis of specific type of interneurons in the OB.

### Transcriptional profiles in adult NSCs with Top2a ablation

To gain insight into the underlying molecular mechanisms of TOP2a function in adult neurogenesis, we performed RNA-Seq analysis in NSCs after down-regulation of TOP2a with PluriSIn#2 (Supplementary Figure S13A). Compared with the DMSO group, the proportion of cultured adult NSC-derived neurospheres with a small size markedly increased in the PluriSIn#2 group, while that with large or middle sizes decreased greatly (Supplementary Figure S13B). These neurospheres were collected for bulk transcriptomic RNA-Seq. As can be seen in Figure 6A, the samples showed excellent consistency with the same group and conspicuous heterogeneity with different treatment. We also found that the RNA expression level of Top2a but not Top2b decreased remarkably, providing further evidence that PluriSIn#2 could specifically and effectively down-regulate Top2a in NSCs (Figure 6B). Compared with the DMSO group, RNA-Seq analysis showed that there were 4363 DEGs in the PluriSIn#2 group, comprising 2594 up-regulated genes and 1769 down-regulated genes (Figure 6C; Supplementary Table S1). It is of note that PluriSIn#2 treatment did not result in significant up-regulation of apoptotic genes (Supplementary Figure S13C). Our study focused on the 1769 down-regulated genes. GO analysis revealed that these genes were mainly involved in the biological process of cell dividing, such as the cell cycle, transcriptional process and mRNA processing (Figure 6D), consistent with the results of KEGG pathway analysis (Supplementary Figure S13D) and gene set enrichment analysis (GSEA) (Supplementary Figure 13E). Of note, the heatmap in Figure 6E showed that the enriched genes were primarily related to cell proliferation and were remarkably down-regulated after PluriSIn#2 treatment. Importantly, PluriSIn#2-mediated Top2a down-regulation significantly decreased the expression level of stem cell-related genes, such as Kif4, Nes, Hes5 and Gsx2, while it obviously increased the expression level of neural differentiation-related genes, such as Gad1, Syp, Rbfox3 and Calb2 (Figure 6F). Taken together, these findings provide molecular evidence that Top2a plays a key role in the proliferation of adult NSCs and that Top2a down-regulation may be detrimental to the maintenance of their stemness property.

### Identification of the direct TOP2a targets by integration of ChIP-Seq and RNA-Seq analysis

To identify putative TOP2a target genes in adult NSCs, we also performed genome-wide ChIP-Seq using specific TOP2a antibody against the C-terminal domain of TOP2a that represents the main differential region from TOP2b (9). Model-based analysis of ChIP-Seq (MACS2, version: 2.1.4) identified 906 significant TOP2a-bound sites (Figure 7A). KEGG annotation showed that the corresponding genes of these bound sites were mostly enriched in the Notch signaling pathway, Hippo signaling pathway or Wnt signaling pathway (Figure 7B). To characterize the regions bound by TOP2a in NSCs, ChIPseek (a bioconductor package) was used to analyze the genome-wide distribution of TOP2a-bound peaks (50). As shown in Figure 7C, most of these peaks were mapped to intron (41.3%) and intergenic regions (37.3%). It is of note that there were 9.2% peaks mapping to the promoter–transcription start site (TSS) $\pm$ 1 kb combined regions, hinting that they might be involved in transcriptional regulation (Figure 7C). In addition, to interpret our ChIP-Seq data within broader regulatory networks, we also searched for transcription factor (TF) motifs among TOP2a-bound sites that mapped within $\pm$ 10 kb of the promoter–TSS (51). The HOMER (version 4.11) *de novo* motif algorithm using 'findMotifsGenome.pl' program with default parameters identified the known TF-binding motifs, such as Tcf12, Ascl1, Sox2 and Sox3 which are closely related to stem cells, suggesting that TOP2a may regulate the activity of NSCs in a transcription-dependent manner (Figure 7D, E).

Next, we combined ChIP-Seq analysis with RNA-Seq analysis to identify candidate targets of TOP2a. As shown in Figure 7F, we superimposed TOP2a ChIP-Seq data with the DEGs from RNA-Seq and identified 724 potential TOP2a target genes that were bound and regulated by TOP2a. Among the potential TOP2a targets, 22.4% of genes (162) were down-regulated after PluriSIn#2 treatment compared with the control (Figure 7F). Furthermore, among the 162 genes, there were 26 genes with TOP2a-binding sites in promoter–TSS regions, indicating that they might be involved in TOP2a-mediated transcriptional regulation. Of these 26 genes, four cell cycle-related genes (Usp37, Birc6, Ddx51 and Gna14) and four stem cell-related genes (Sox2, Hes5, Nup153 and Nup133) were validated by ChIP-qPCR and confirmed by RNA-Seq expression data (Figure 7G). The binding of these eight genes with TOP2a was also validated by genome track analysis (Figure 7H; Supplementary Figure S14). Based on a literature review and evaluation, we focused on three candidate TOP2a target genes, Usp37, Sox2 and Hes5, for further analysis. When their expression in NSCs was knocked down by lentivirus-mediated interference, we found that only Usp37 knockdown could impede the self-renewal of NSCs *in vitro* (Supplementary Figure S15), suggesting that Usp37 is one of the most likely direct genomic targets of TOP2a.

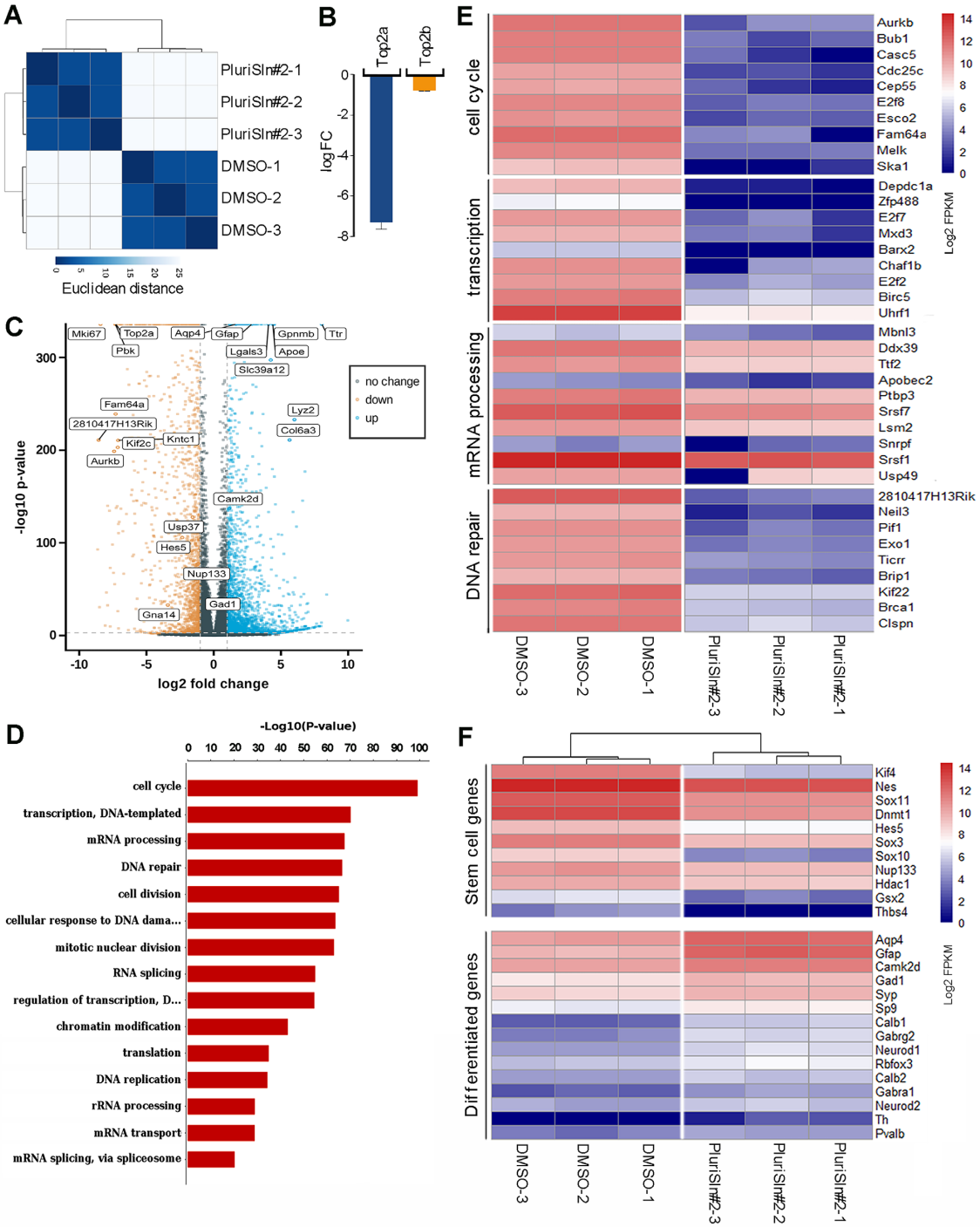


**Figure 6.** Transcriptional changes in adult NSCs after Top2a down-regulation. (**A**) Heatmap of the sample-to-sample Euclidian distances shows the dataset structure and high replicate concordance. (**B**) The gene expression changes of Top2a and Top2b in the RNA-Seq (mean ± SEM, $n = 3$). (**C**) Dotplot shows the DEGs between the DMSO and PluriSIn#2 group in RNA-Seq. |log2FC| >1 and FDR <0.05 were used as the cut-off. Some interesting genes are indicated. (**D**) GO analysis of the down-regulated genes. (**E**) Heatmap illustrating the normalized expression of enriched genes in GO terms in (D). (**F**) Heatmap illustrating the normalized expression of stem cell genes and differentiated genes in NSCs.

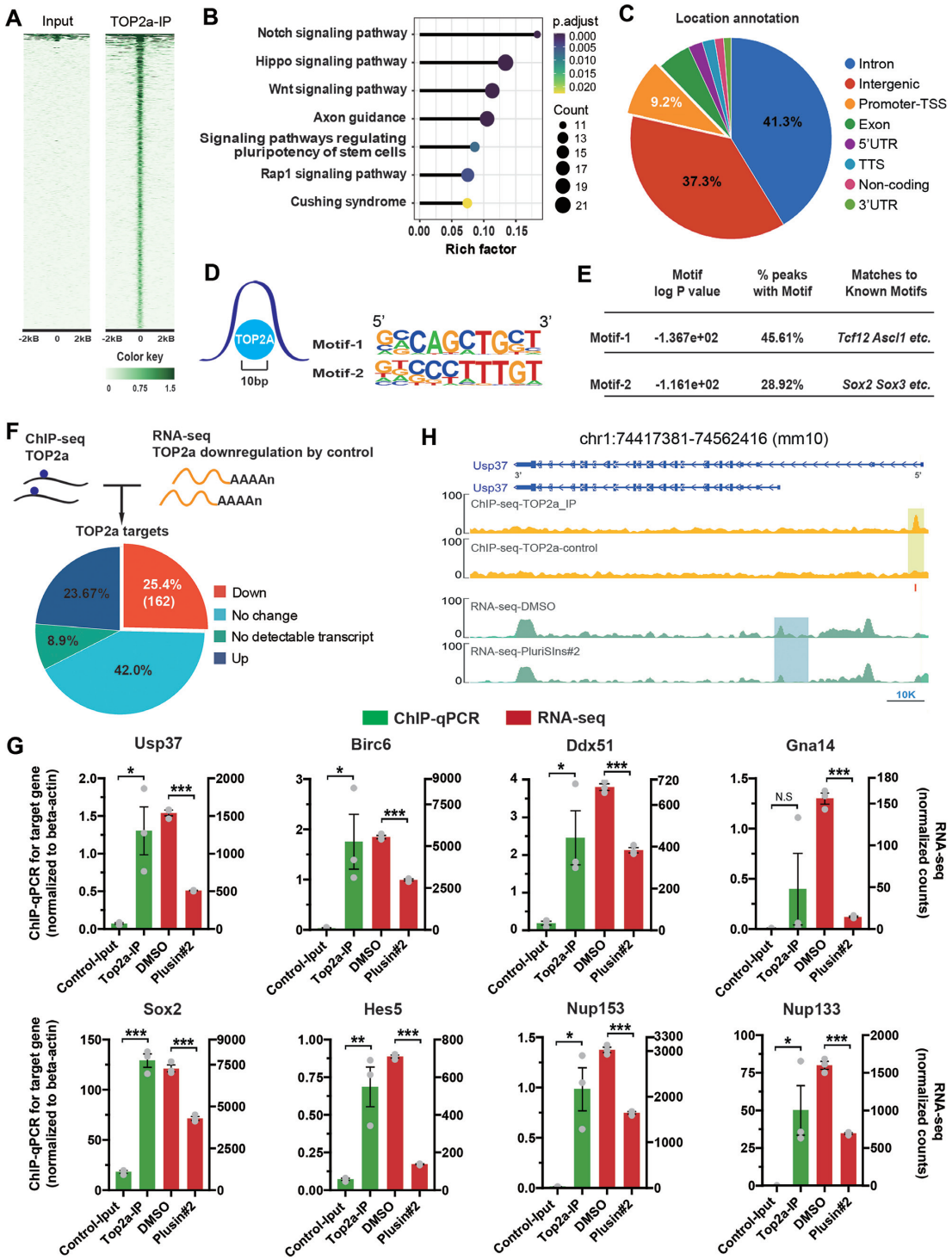


**Figure 7.** Integrating the ChIP-Seq and RNA-Seq data to identify potential direct downstream targets of TOP2a in adult NSCs. (**A**–**E**) ChIP-Seq analysis using TOP2a antibody. (A) Heatmaps of TOP2a ChIP-Seq peaks (total number: 906). (B) Annotation of peak-related genes by KEGG pathway analysis. Rich factor refers to the percentage of mapped genes in all genes of one certain pathway set. (C) Genomic distribution of TOP2a binding categorized based on the associated type of genomic region. (D) The top two binding motifs of TOP2a. (E) *De novo* HOMER analysis with default parameters for identification of TOP2a motifs. *P*-value ≤1e-50 was set as the criterion for screening of the most significant motifs. Detailed information on motif 1 and motif 2 is provided in Supplementary file S1 and S2, respectively. In addition, a full list of motif analysis and selection is provided in Supplementary file S3. (**F**–**H**) Identifying potential direct TOP2a targets. (F) Distribution of gene expression changes associated with TOP2a-binding sites annotated to the nearest genes using HOMER and RNA-Seq data in the Top2a down-regulation and control group. (G) The candidate genes, including cell cycle-related genes (Usp37, Birc6, Ddx51 and Gna14) and stem cell-related genes (Sox2, Hes5, Nup153 and Nup133), were validated by ChIP-qPCR and confirmed by RNA-Seq expression data. Data are plotted as the mean ± SEM. N.S., $P \geq 0.05$, *$P < 0.05$, **$P < 0.01$, ***$P < 0.01$ by Student's *t*-test. All experiments were performed at least three times independently. (H) Representative genome tracks showing a TOP2a-bound peak and expression change of the candidate direct target gene Usp37. Relevant loci showing TOP2a ChIP-Seq (orange) and RNA-Seq (cyan) results are based on the Bigwig files.

### TOP2a promotes NSC proliferation via Usp37

USP37 is a novel member of ubiquitin-specific processing proteases that can prevent ubiquitin-mediated degradation of target proteins. By mediating deubiquitination of CYCLIN-A (including CCNA1 and CCNA2), USP37 serves as a potent regulator of the cell cycle, promoting $G_1$/S transition with exceptionally high expression (52). In addition, USP37 also plays a critical role in the regulation of DNA replication by stabilizing the licensing factor CDT1 (53). By immunostaining, we found that USP37 was expressed in adult brain SVZ NSCs (Supplementary Figure S16A) and cultured adult NSCs (Supplementary Figure S16B). When NSCs were infected with Usp37-expressing lentivirus, it resulted in USP37 overexpression in these cells (Supplementary Figure S16C, D). Of note, USP37 overexpression enhanced the proliferation of NSCs in neurospheres (Supplementary Figure S16E, F), which significantly increased the number and diameter of NSC-formed neurospheres (Supplementary Figure S16G, H). Next, we constructed three shRNAs (shRNA1–3) against Usp37 in the lentiviral vectors in which the gene expression was driven by the hGFAP promoter and the co-expressed GFP was used as the reporter. Among these three shRNAs, western blotting showed that shRNA3 was qualified for the efficient interference of Usp37 in NSCs (Supplementary Figure S17A, B). Therefore, shRNA3 (indicated by Usp37-shRNA) was used in the subsequent experiments. In contrast to USP37 overexpression, Usp37 knocked down by shRNA resulted in a significant decrease in the number and diameter of neurospheres formed by NSCs (Supplementary Figure S17C, D), consistent with the results of Top2a knockdown (Figure 2D, E).

To investigate whether USP37 overexpression can rescue the impaired self-renewal ability of adult NSCs caused by Top2a knockdown, we infected NSCs with Usp37-overexpressing (Usp37-OE) lentivirus immediately after Top2a knockdown by shRNA (Top2a-shRNA). Western blotting analysis revealed that the expression of USP37 decreased synchronously under the condition of Top2a knockdown, providing further evidence that Usp37 was a direct target gene of TOP2a (Figure 8A–C). The known USP37 targets, CDT1 and CYCLIN-A, were also detected. Figure 8A and D showed that Top2a knockdown failed to reduce CDT1 expression significantly. However, the expression of CYCLIN-A, a classical participator in regulation of the cell cycle, was markedly down-regulated, suggesting that it is under the control of Top2a (Figure 8A, E). Of note, when USP37 was overexpressed in NSCs, the expression of CYCLIN-A was not reversed significantly ($P = 0.10$) (Figure 8A, E), while the number and diameter of neurospheres decreased by Top2a knockdown were rescued to a considerable level (Figure 8F, G). We supposed that Usp37 might maintain the self-renewal and proliferation of NSCs by stabilization of the CYCLIN-A protein. In addition, we injected Usp37-overexpressing lentivirus into the SVZ of adult CKO mice (Nestin::Top2a$^{F/F}$). Seven days later, immunohistochemical analysis showed that the proliferative activity of SVZ NSCs increased with Usp37 overexpression and the Top2a knockout-induced impaired neurogenesis (indicated by DCX staining) was significantly rescued in the SVZ (Figure 8H, I). Altogether, these data indicate that Usp37 functions as a direct target of TOP2a and is involved in tuning the proliferative activity of adult NSCs with a high dependence on TOP2a.

## DISCUSSION

Since adult neurogenesis was first observed in the 1960s, it has grown into an important topic in a variety of research fields. Although the maintenance of adult NSCs and the generation of their progeny are absolutely indispensable for further adult neurogenesis, the underlying molecular mechanisms remain largely unknown. While TOP2a has been well established as a nuclear enzyme that resolves torsional stress of DNA, little is known about its function in genomic transcriptional regulation, especially during adult neurogenesis. In this study, we provide proof-of-principle evidence suggesting that TOP2a is exclusively expressed in adult stem/progenitor cells in the SVZ, including activated NSCs, TAPs and NBs, and plays a key role in adult neurogenesis by regulating a set of genes in a transcription-dependent manner. Importantly, for the first time, we identified a deubiquitinase, Usp37, as a direct genomic downstream effector of TOP2a.

### Region-restricted expression pattern of TOP2a in adult brains

In terms of the expression features of TOP2, in 1992, Capranico *et al*. showed that TOP2a was mainly expressed in proliferating tissues in adult mice, such as bone marrow, spleen and intestine, while they did not detect TOP2a expression in the brain (54). Harkin *et al*. investigated the expression patterns of TOP2 in the early fetal human telencephalon between 9 and 12 post-conception weeks, finding that TOP2a was restricted to the cells in proliferative layers of the cortex and ganglionic eminences (GEs), including the VZ and SVZ (55). These results are consistent with our findings on the expression pattern of TOP2a in the brain of embryonic and post-natal mice. In adult mice, strikingly, we found that unlike TOP2b, which was widely distributed in the brain, TOP2a was exclusively expressed in the neurogenic niches, especially in the SVZ. Of note, TOP2a was shown to be preferentially expressed in the dlSVZ and vSVZ, indicating that TOP2a might be a region-specific regulator of NSCs in adult neurogenesis. Immunohistochemical analysis further confirmed that these TOP2a-positive cells in the SVZ were NSCs, TAPs and NBs. Almost all TOP2a-expressing cells were immunoreactive for PCNA and labeled by BrdU in the short-term labeling experiments. Moreover, although TOP2a was expressed in GFAP$^+$, NESTIN$^+$ or SOX2$^+$ NSCs, these cells were not labeled by BrdU in the long-term label-retention experiments, suggestive of activated but not quiescent NSCs. Therefore, all these findings indicate that TOP2a is exclusively expressed in activated NSCs, TAPs and NBs, which represent the actively proliferating stem/progenitor cells in the SVZ. Importantly, quantitative analysis of the expression pattern in the SVZ–RMS–OB system revealed that the number of TOP2a$^+$ cells declined with the distance from the SVZ. TOP2a protein begins to be expressed when quiescent

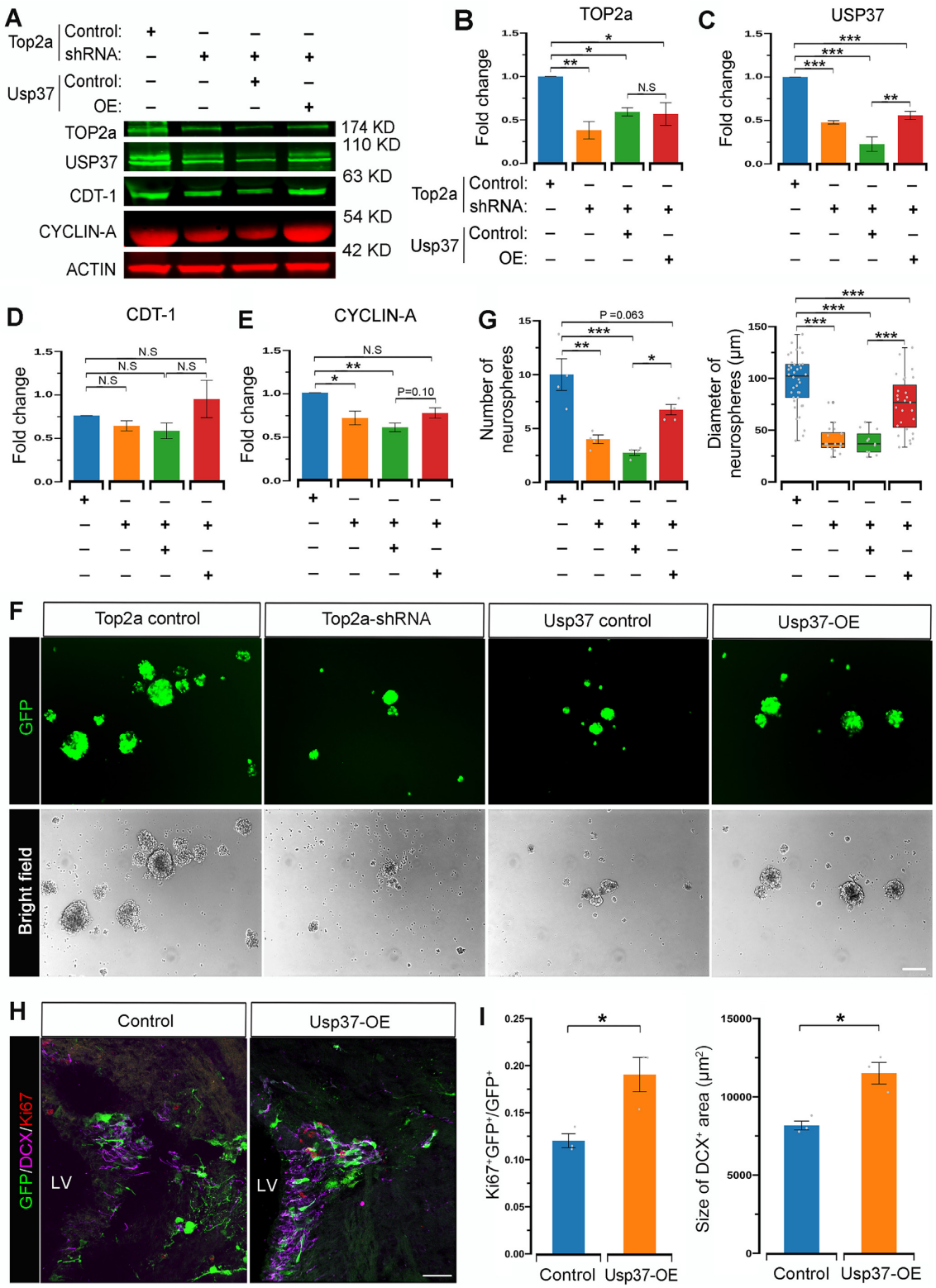


**Figure 8.** Overexpression of Usp37 is sufficient to rescue the impaired self-renewal ability of adult NSCs caused by Top2a knockdown or knockout. (**A**–**E**) Western blotting was performed to analyze the expression of TOP2a, USP37, CDT-1 and CYCLIN-A in NSCs after Top2a knockdown (shRNA) or/and Usp37 overexpression (OE). Data from (A) were quantified in (B–E). (**F** and **G**) Quantitative analysis of the number and diameter of NSC-formed neurospheres after Top2a knockdown or/and Usp37 overexpression. (**H** and **I**) Immunohistochemical analysis showed that Usp37 overexpression is sufficient to rescue the impaired proliferative activity and adult neurogenesis caused by Top2a knockout. The control or Usp37-expressing (Usp37-OE) lentivirus was injected into the SVZ of adult Nestin::Top2a$^{F/F}$ mice after tamoxifen induction. Data are plotted as mean ± SEM. N.S., $P \geq 0.05$, *$P < 0.05$, **$P < 0.01$, ***$P < 0.01$ by one-way ANOVA with Tukey's post-hoc test (B–E and G) or Student's *t*-test (I). All experiments were performed at least three times independently. The scale bars represent 100 μm (F) and 40 μm (H).

NSCs become activated and differentiate into proliferating TAPs and NBs, while it decreases during the migration in the RMS and eventually disappears in the deep layers of the OB. This dynamic spatial expression pattern may be explained by a previous study that showed a switch in the expression from TOP2a to TOP2b during the differentiation of NSCs into neurons (10,11). Collectively, all these findings hint that TOP2a may play a key role in adult neurogenesis.

In addition, we examined the expression of TOP2a in ependymal cells lining the LV, a type of cell that may contribute to the neurogenesis after brain insults, including ischemia and inflammatory diseases (56,57). However, we failed to find any TOP2a expression in these cells under physiological conditions. Future studies are needed to elucidate whether TOP2a appears in ependymal cells in pathological conditions. Of note, we detected considerable $TOP2a^+$ cells located in the DG of the hippocampus, another neurogenic niche in adult brains. Whether TOP2a plays a role in adult hippocampal neurogenesis should be determined in future studies.

### Role of TOP2a in the maintenance of adult neurogenesis

As a traditional nuclear enzyme that resolves torsional stress of DNA, TOP2a has been well documented in the field of cancer research and identified as a critical target for anticancer drugs (58). However, the functions of TOP2a in the nervous system remain unknown, especially in adult neurogenesis. The NSCs residing in the SVZ are characterized by the abilities to self-renew and produce the functional neurons in the brain (48). Therefore, we first examined whether blocking TOP2a affected the self-renewal and proliferation of adult NSCs. When TOP2a was knocked down by shRNA or chemically down-regulated by PluriSIn#2, there was a significant reduction in the number and diameter of neurospheres cultured from SVZ-derived NSCs, indicative of a critical role for TOP2a in the self-renewal and proliferation of SVZ-derived NSCs.

Based on the findings *in vitro*, we next investigated the role of TOP2a in adult NSCs in the SVZ. Because Top2a deletion is lethal in mice at the embryonic stage (12), we generated transgenic mice with the CreERT2/loxP recombination system to conditionally knock out Top2a in adulthood, in which SVZ NSCs were specifically targeted by Nestin::CreERT2- or Gfap::CreERT2-mediated combination. Interestingly, we found that selective deletion of Top2a resulted in a significant decrease in the number of activated NSCs in the SVZ, while it had no effect on quiescent NSCs. This finding is consistent with the expression pattern, namely that Top2a was expressed in activated NSCs but not quiescent NSCs in the SVZ. As the progeny cells of activated NSCs, we also observed that the number of TAPs and NBs in the SVZ was reduced markedly in Top2a knockout mice. In the adult brain, NBs continuously generated in the SVZ migrate rapidly through the RMS to the OB, where they give rise to two types of interneurons, i.e. granule cells (GCs) and periglomerular cells (PGCs). These adult-born OB interneurons located in the GCL and GL express specific markers, including CR, CB, PV and TH. Of note, different SVZ regions contribute to the heterogeneity of OB interneurons. The dorsal SVZ primarily produces superficial GCs and $TH^+$ PGCs, while the ventral SVZ mostly generates deep GCs and $CB^+$ PGCs (59). Additionally, the RMS also produces $CR^+$ interneurons in both the GCL and GL (59). Because the expression pattern showed that TOP2a was mainly expressed in the dlSVZ, vSVZ and RMS, we next examined whether conditional knockout of Top2a affected the generation of OB interneurons. However, we failed to find any significant changes in the number of different subtypes of interneurons in the GCL and GL of the OB after the selective deletion of Top2a in NSCs. Considering that SVZ-derived newborn neurons only account for a small proportion of the total OB interneurons, we then performed immunohistochemical analysis of the BrdU-traced newborn interneurons in the OB. Intriguingly, we revealed that the conditional ablation of Top2a in NSCs resulted in a remarkable loss of $CB^+$ and $CR^+$ newly generated OB interneurons. All these data suggest that TOP2a is required for the maintenance of adult neurogenesis in the SVZ–RMS–OB system. Besides, given that TOP2a is an important target for antitumor drugs that have been widely used in antitumor therapy, more attention should be paid to the possible side effects of TOP2a down-regulation on normal adult neurogenesis.

### Usp37 serves as a direct TOP2a target mediating the transcriptional regulation scheme in adult NSCs

To uncover the molecular mechanisms underlying TOP2a function in adult neurogenesis, RNA-Seq and ChIP-Seq analyses were performed in adult NSCs after down-regulation of Top2a by PluriSIn#2. Using RNA-Seq analysis, we screened out a series of DEGs mainly related to stemness and the cell cycle, suggestive of a powerful transcriptional regulatory role for TOP2a in NSCs. We speculated that TOP2a might be able to initiate the transcription of these genes in NSCs for progress of adult neurogenesis in the SVZ, which is a novel function for TOP2a distinct from its traditional activity as a nuclear enzyme to relieve torsional stress of DNA. This is also in agreement with the reports that TOP2 could change the structure of chromatin and facilitate the binding of a massive number of TFs to the target genes during transcription (10,60–63), which might be modulated by the C-terminal domains of TOP2a and under the control of tyrosyl-DNA phosphodiesterase 2 (TDP2) hydrolase activity (9,64,65). Using ChIP-Seq analysis, we found a group of potential direct TOP2a target genes containing the binding site at the promoter regions, indicating that they might be engaged in transcriptional regulation. Integrating the RNA-Seq and ChIP-Seq analyses, we identified 26 direct candidate TOP2a targets, including Usp37, Nup153, Nup133, Sox2, Hes5, Birc6, Ddx51 and Gna14. Among these candidate target genes, gain-of-function and loss-of-function analyses confirmed that Usp37 was involved in TOP2a-mediated transcriptional regulation in NSCs. Importantly, overexpression of Usp37 was sufficient to rescue the effect of Top2a knockdown on NSCs. Of note, the majority of peaks from TOP2a ChIP-Seq were intergenic or intronic, suggestive of a relationship with 3D genome folding. Interestingly, both TOP1 and TOP2b have been reported to coordinate the transcriptional activation by participating in RNA polymerase II

promoter-proximal pausing and DSB enrichment (66,67). Therefore, we think that the 3D genome folding may jointly contribute to the role of TOP2a in transcriptional regulation, although further studies are necessary.

The deubiquitinating enzyme family has been shown to antagonize the ubiquitin–proteasome system and thereby maintain the equilibrium between ubiquitination and deubiquitination reactions (68,69). Indeed, almost all aspects of cell biological processes, including the cell cycle, are controlled by the post-translational conjugation of ubiquitin (70). Ubiquitination is reversible, and ubiquitin can be removed from substrates by catalytic proteases termed deubiquitinases. USP27x and its homologs USP22 and USP51 have been reported to deubiquitinate and stabilize Hes1, and thereby coordinatively regulate neuronal differentiation via Notch signaling in the mouse developing brain (71). USP37 is a novel member of the deubiquitinating enzyme family that can block ubiquitin-mediated degradation of target proteins by deubiquitination (70,72). It plays a key role in DNA damage resistance. For example, USP37 was identified as an important modulator of the sensitivity to camptothecin, a drug used for cancer therapeutics (73). Of note, USP37 was shown to regulate stemness-related genes in cancer stem cells. For example, USP37 could regulate the stemness and cell invasion in breast cancer (74). In lung cancer, USP37 was found to directly bind the pluripotent factor C-MYC protein and regulate its stability (75). In addition, it has been well documented that the established stem cell marker SOX2 has a robust regulatory role in neurogenesis (76,77). Intriguingly, USP37 was reported to control the transcriptional level of SOX2 by binding with its promoter region (72). CDT1 and CYCLIN-A are two well-known regulators of mitotic division in the cell, and they can be stabilized by USP37 via deubiquitination (52,53). In our study, the protein level of CYCLIN-A but not CDT-1 was roughly synchronized with that of USP37 in NSCs. All these data suggest that Usp37 in NSCs is transcriptionally controlled by TOP2a and mediates its role in adult neurogenesis via CYCLIN-A.

In summary, our work demonstrates that TOP2a exerts a powerful homeostatic role in maintaining NSC activity for sustainable adult neurogenesis, which is mediated by transcriptional activation of its direct target Usp37.

## DATA AVAILABILITY

ChIP-Seq: GEO accession GSE192397. RNA-Seq: GEO accession GSE192398.

## SUPPLEMENTARY DATA

Supplementary Data are available at NAR Online.

## ACKNOWLEDGEMENTS

We are particularly grateful to Professor Luonan Chen from the Chinese Academy Sciences for the technical support in bioinformatics analysis and would like to thank Professor Zhengang Yang from Fudan University for critical reading of the manuscript. We thank LetPub (www.letpub.com) for its linguistic assistance during the preparation of this manuscript.

*Author contributions:* S.Q., Y.Y., C.H. and Z.S. conceived and designed the experiments. S.Q., Y.Y., X.H., Z.T., X.H., H.L. and Y.P. performed the experiments. S.Q., Y.Y., C.H. and Z.S. analyzed the data and prepared the manuscript. All authors reviewed and approved the manuscript.

## FUNDING

The Ministry of Science and Technology China Brain Initiative Grant (2022ZD0204702); the National Natural Science Foundation (81971161, 82171386, 31871026, 82002012); the Shanghai Science and Technology Development Funds (22YF1458600); the Foundation from Naval Medical University (2021QN08); the Shanghai Municipal Science and Technology Major Project (No.2018SHZDZX01), ZJ Lab, and Shanghai Center for Brain Science and Brain-Inspired Technology. Funding for open access charge: Ministry of Science and Technology China Brain Initiative and National Natural Science Foundation of China.

*Conflict of interest statement.* None declared.

## REFERENCES

1. Vos,S.M., Tretter,E.M., Schmidt,B.H. and Berger,J.M. (2011) All tangled up: how cells direct, manage and exploit topoisomerase function. *Nat. Rev. Mol. Cell Biol.*, **12**, 827–841.
2. Ashour,M.E., Atteya,R. and El-Khamisy,S.F. (2015) Topoisomerase-mediated chromosomal break repair: an emerging player in many games. *Nat. Rev. Cancer*, **15**, 137–151.
3. Dehshahri,A., Ashrafizadeh,M., Ghasemipour Afshar,E., Pardakhty,A., Mandegary,A., Mohammadinejad,R. and Sethi,G. (2020) Topoisomerase inhibitors: pharmacology and emerging nanoscale delivery systems. *Pharmacol. Res.*, **151**, 104551.
4. McKie,S.J., Maxwell,A. and Neuman,K.C. (2020) Mapping DNA topoisomerase binding and cleavage genome wide using next-generation sequencing techniques. *Genes (Basel)*, **11**, 92.
5. Wang,J.C. (2002) Cellular roles of DNA topoisomerases: a molecular perspective. *Nat. Rev. Mol. Cell Biol.*, **3**, 430–440.
6. Corbett,K.D. and Berger,J.M. (2004) Structure, molecular mechanisms, and evolutionary relationships in DNA topoisomerases. *Annu. Rev. Biophys. Biomol. Struct.*, **33**, 95–118.
7. Champoux,J.J. (2001) DNA topoisomerases: structure, function, and mechanism. *Annu. Rev. Biochem.*, **70**, 369–413.
8. Kroll,D.J. (1997) Homologous and heterologous protein–protein interactions of human DNA topoisomerase IIalpha. *Arch. Biochem. Biophys.*, **345**, 175–184.
9. Kozuki,T., Chikamori,K., Surleac,M.D., Micluta,M.A., Petrescu,A.J., Norris,E.J., Elson,P., Hoeltge,G.A., Grabowski,D.R., Porter,A.C.G. *et al.* (2017) Roles of the C-terminal domains of topoisomerase IIalpha and topoisomerase IIbeta in regulation of the decatenation checkpoint. *Nucleic Acids Res.*, **45**, 5995–6010.
10. Thakurela,S., Garding,A., Jung,J., Schübeler,D., Burger,L. and Tiwari,V.K. (2013) Gene regulation and priming by topoisomerase IIα in embryonic stem cells. *Nat. Commun.*, **4**, 2478.
11. Tiwari,V.K., Burger,L., Nikoletopoulou,V., Deogracias,R., Thakurela,S., Wirbelauer,C., Kaut,J., Terranova,R., Hoerner,L., Mielke,C. *et al.* (2012) Target genes of topoisomerase IIbeta regulate neuronal survival and are defined by their chromatin state. *Proc. Natl Acad. Sci. USA*, **109**, E934–E943.
12. Akimitsu,N., Adachi,N., Hirai,H., Hossain,M.S., Hamamoto,H., Kobayashi,M., Aratani,Y., Koyama,H. and Sekimizu,K. (2003) Enforced cytokinesis without complete nuclear division in embryonic cells depleting the activity of DNA topoisomerase IIalpha. *Genes Cells*, **8**, 393–402.
13. Carpenter,A.J. and Porter,A.C. (2004) Construction, characterization, and complementation of a conditional-lethal DNA topoisomerase IIalpha mutant human cell line. *Mol. Biol. Cell*, **15**, 5700–5711.

14. Gothe,H.J., Bouwman,B.A.M., Gusmao,E.G., Piccinno,R., Petrosino,G., Sayols,S., Drechsel,O., Minneker,V., Josipovic,N., Mizi,A. *et al.* (2019) Spatial chromosome folding and active transcription drive DNA fragility and formation of oncogenic MLL translocations. *Mol. Cell*, **75**, 267–283.
15. Baranello,L., Kouzine,F. and Levens,D. (2013) DNA topoisomerases beyond the standard role. *Transcription*, **4**, 232–237.
16. Gage,F.H. (2019) Adult neurogenesis in mammals. *Science*, **364**, 827–828.
17. Santarelli,L., Saxe,M., Gross,C., Surget,A., Battaglia,F., Dulawa,S., Weisstaub,N., Lee,J., Duman,R., Arancio,O. *et al.* (2003) Requirement of hippocampal neurogenesis for the behavioral effects of antidepressants. *Science*, **301**, 805–809.
18. Clelland,C.D., Choi,M., Romberg,C., Clemenson,G.D.,Jr., Fragniere,A., Tyers,P., Jessberger,S., Saksida,L.M., Barker,R.A., Gage,F.H *et al.* (2009) A functional role for adult hippocampal neurogenesis in spatial pattern separation. *Science*, **325**, 210–213.
19. Sahay,A., Scobie,K.N., Hill,A.S., O'Carroll,C.M., Kheirbek,M.A., Burghardt,N.S., Fenton,A.A., Dranovsky,A. and Hen,R. (2011) Increasing adult hippocampal neurogenesis is sufficient to improve pattern separation. *Nature*, **472**, 466–470.
20. Mukherjee,S., Brulet,R., Zhang,L. and Hsieh,J. (2016) REST regulation of gene networks in adult neural stem cells. *Nat. Commun.*, **7**, 13360.
21. Montalbán-Loro,R., Lozano-Ureña,A., Ito,M., Krueger,C., Reik,W., Ferguson-Smith,A.C. and Ferrón,S.R. (2019) TET3 prevents terminal differentiation of adult NSCs by a non-catalytic action at snrpn. *Nat. Commun.*, **10**, 1726.
22. Kjell,J., Fischer-Sternjak,J., Thompson,A.J., Friess,C., Sticco,M.J., Salinas,F., Cox,J., Martinelli,D.C., Ninkovic,J., Franze,K. *et al.* (2020) Defining the adult neural stem cell niche proteome identifies key regulators of adult neurogenesis. *Cell Stem Cell*, **26**, 277–293.
23. Fletcher,R.B., Prasol,M.S., Estrada,J., Baudhuin,A., Vranizan,K., Choi,Y.G. and Ngai,J. (2011) p63 regulates olfactory stem cell self-renewal and differentiation. *Neuron*, **72**, 748–759.
24. Wang,H., Kane,A.W., Lee,C. and Ahn,S. (2014) Gli3 repressor controls cell fates and cell adhesion for proper establishment of neurogenic niche. *Cell Rep.*, **8**, 1093–1104.
25. Heng,X. and Le,W.D. (2010) The function of DNA topoisomerase IIbeta in neuronal development. *Neurosci. Bull.*, **26**, 411–416.
26. Guo,W., Patzlaff,N.E., Jobe,E.M. and Zhao,X. (2012) Isolation of multipotent neural stem or progenitor cells from both the dentate gyrus and subventricular zone of a single adult mouse. *Nat. Protoc.*, **7**, 2005–2012.
27. Su,Z., Niu,W., Liu,M.L., Zou,Y. and Zhang,C.L. (2014) In vivo conversion of astrocytes to neurons in the injured adult spinal cord. *Nat. Commun.*, **5**, 3338.
28. Wang,C., Liang,C.C., Bian,Z.C., Zhu,Y. and Guan,J.L. (2013) FIP200 is required for maintenance and differentiation of postnatal neural stem cells. *Nat. Neurosci.*, **16**, 532–542.
29. Su,Z., Yuan,Y., Cao,L., Zhu,Y., Gao,L., Qiu,Y. and He,C. (2010) Triptolide promotes spinal cord repair by inhibiting astrogliosis and inflammation. *Glia*, **58**, 901–915.
30. Dobin,A., Davis,C.A., Schlesinger,F., Drenkow,J., Zaleski,C., Jha,S., Batut,P., Chaisson,M. and Gingeras,T.R. (2013) STAR: ultrafast universal RNA-seq aligner. *Bioinformatics*, **29**, 15–21.
31. Love,M.I., Huber,W. and Anders,S. (2014) Moderated estimation of fold change and dispersion for RNA-seq data with DESeq2. *Genome Biol.*, **15**, 550.
32. Anders,S., Pyl,P.T. and Huber,W. (2015) HTSeq—a python framework to work with high-throughput sequencing data. *Bioinformatics*, **31**, 166–169.
33. Yu,G., Wang,L.G., Han,Y. and He,Q.Y. (2012) clusterProfiler: an R package for comparing biological themes among gene clusters. *OMICS*, **16**, 284–287.
34. Li,H. and Durbin,R. (2009) Fast and accurate short read alignment with Burrows–Wheeler transform. *Bioinformatics*, **25**, 1754–1760.
35. Zhang,Y., Liu,T., Meyer,C.A., Eeckhoute,J., Johnson,D.S., Bernstein,B.E., Nusbaum,C., Myers,R.M., Brown,M., Li,W. *et al.* (2008) Model-based analysis of chip-Seq (MACS). *Genome Biol.*, **9**, R137.
36. Heinz,S., Benner,C., Spann,N., Bertolino,E., Lin,Y.C., Laslo,P., Cheng,J.X., Murre,C., Singh,H. and Glass,C.K. (2010) Simple combinations of lineage-determining transcription factors prime cis-regulatory elements required for macrophage and b cell identities. *Mol. Cell*, **38**, 576–589.
37. Lopez-Juarez,A., Howard,J., Ullom,K., Howard,L., Grande,A., Pardo,A., Waclaw,R., Sun,Y.Y., Yang,D., Kuan,C.Y. *et al.* (2013) Gsx2 controls region-specific activation of neural stem cells and injury-induced neurogenesis in the adult subventricular zone. *Genes Dev.*, **27**, 1272–1287.
38. Götz,M., Nakafuku,M. and Petrik,D. (2016) Neurogenesis in the developing and adult brain—similarities and key differences. *Cold Spring Harb. Perspect. Biol.*, **8**, a018853.
39. Bonaguidi,M.A., Wheeler,M.A., Shapiro,J.S., Stadel,R.P., Sun,G.J., Ming,G.-l. and Song,H. (2011) In vivo clonal analysis reveals self-renewing and multipotent adult neural stem cell characteristics. *Cell*, **145**, 1142–1155.
40. Li,X., Liu,G., Yang,L., Li,Z., Zhang,Z., Xu,Z., Cai,Y., Du,H., Su,Z., Wang,Z. *et al.* (2021) Decoding cortical glial cell development. *Neurosci. Bull.*, **37**, 440–460.
41. Mizrak,D., Bayin,N.S., Yuan,J., Liu,Z., Suciu,R.M., Niphakis,M.J., Ngo,N., Lum,K.M., Cravatt,B.F., Joyner,A.L. *et al.* (2020) Single-cell profiling and SCOPE-Seq reveal lineage dynamics of adult ventricular–subventricular zone neurogenesis and NOTUM as a key regulator. *Cell Rep.*, **31**, 107805.
42. Xie,T. (2009) Stem cell in the adult drosophila hindgut: just a sleeping beauty. *Cell Stem Cell*, **5**, 227–228.
43. Ben-David,U., Cowell,I.G., Austin,C.A. and Benvenisty,N. (2015) Brief reports: controlling the survival of human pluripotent stem cells by small molecule-based targeting of topoisomerase II alpha. *Stem Cells*, **33**, 1013–1019.
44. Baxter,J. and Diffley,J.F. (2008) Topoisomerase II inactivation prevents the completion of DNA replication in budding yeast. *Mol. Cell*, **30**, 790–802.
45. Nielsen,C.F., Zhang,T., Barisic,M., Kalitsis,P. and Hudson,D.F. (2020) Topoisomerase IIalpha is essential for maintenance of mitotic chromosome structure. *Proc. Natl Acad. Sci. USA*, **117**, 12131–12142.
46. Pastrana,E., Cheng,L.C. and Doetsch,F. (2009) Simultaneous prospective purification of adult subventricular zone neural stem cells and their progeny. *Proc. Natl Acad. Sci. USA*, **106**, 6387–6392.
47. Zywitza,V., Misios,A., Bunatyan,L., Willnow,T.E. and Rajewsky,N. (2018) Single-cell transcriptomics characterizes cell types in the subventricular zone and uncovers molecular defects impairing adult neurogenesis. *Cell Rep.*, **25**, 2457–2469.
48. Lim,D.A. and Alvarez-Buylla,A. (2016) The adult ventricular–subventricular zone (V-SVZ) and olfactory bulb (OB) neurogenesis. *Cold Spring Harb. Perspect. Biol.*, **8**, a018820.
49. Braun,S.M.G. and Jessberger,S. (2014) Adult neurogenesis: mechanisms and functional significance. *Development*, **141**, 1983–1986.
50. Yu,G., Wang,L.-G. and He,Q.-Y. (2015) ChIPseeker: an R/Bioconductor package for ChIP peak annotation, comparison and visualization. *Bioinformatics*, **31**, 2382–2383.
51. MacIsaac,K.D., Lo,K.A., Gordon,W., Motola,S., Mazor,T. and Fraenkel,E. (2010) A quantitative model of transcriptional regulation reveals the influence of binding location on expression. *PLoS Comput. Biol.*, **6**, e1000773.
52. Huang,X., Summers,M.K., Pham,V., Lill,J.R., Liu,J., Lee,G., Kirkpatrick,D.S., Jackson,P.K., Fang,G. and Dixit,V.M. (2011) Deubiquitinase USP37 is activated by CDK2 to antagonize APC(CDH1) and promote S phase entry. *Mol. Cell*, **42**, 511–523.
53. Hernandez-Perez,S., Cabrera,E., Amoedo,H., Rodriguez-Acebes,S., Koundrioukoff,S., Debatisse,M., Mendez,J. and Freire,R. (2016) USP37 deubiquitinates cdt1 and contributes to regulate DNA replication. *Mol. Oncol.*, **10**, 1196–1206.
54. Capranico,G., Tinelli,S., Austin,C.A., Fisher,M.L. and Zunino,F. (1992) Different patterns of gene expression of topoisomerase II isoforms in differentiated tissues during murine development. *Biochim. Biophys. Acta*, **1132**, 43–48.
55. Harkin,L.F., Gerrelli,D., Gold Diaz,D.C., Santos,C., Alzu'bi,A., Austin,C.A. and Clowry,G.J. (2016) Distinct expression patterns for type II topoisomerases IIA and IIB in the early foetal human telencephalon. *J. Anat.*, **228**, 452–463.
56. Pourabdolhossein,F., Gil-Perotin,S., Garcia-Belda,P., Dauphin,A., Mozafari,S., Tepavcevic,V., Manuel Garcia Verdugo,J. and Baron-Van Evercooren,A. (2017) Inflammatory demyelination

induces ependymal modifications concomitant to activation of adult (SVZ) stem cell proliferation. *Glia*, **65**, 756–772.
57. Li,Y., Chen,J. and Chopp,M. (2002) Cell proliferation and differentiation from ependymal, subependymal and choroid plexus cells in response to stroke in rats. *J. Neurol. Sci.*, **193**, 137–146.
58. Nitiss,J.L. (2009) Targeting DNA topoisomerase II in cancer chemotherapy. *Nat. Rev. Cancer*, **9**, 338–350.
59. Lledo,P.M., Merkle,F.T. and Alvarez-Buylla,A. (2008) Origin and function of olfactory bulb interneuron diversity. *Trends Neurosci.*, **31**, 392–400.
60. Dykhuizen,E.C., Hargreaves,D.C., Miller,E.L., Cui,K., Korshunov,A., Kool,M., Pfister,S., Cho,Y.-J., Zhao,K. and Crabtree,G.R. (2013) BAF complexes facilitate decatenation of DNA by topoisomerase IIα. *Nature*, **497**, 624–627.
61. King,I.F., Yandava,C.N., Mabb,A.M., Hsiao,J.S., Huang,H.S., Pearson,B.L., Calabrese,J.M., Starmer,J., Parker,J.S., Magnuson,T. *et al.* (2013) Topoisomerases facilitate transcription of long genes linked to autism. *Nature*, **501**, 58–62.
62. Madabhushi,R., Gao,F., Pfenning,A.R., Pan,L., Yamakawa,S., Seo,J., Rueda,R., Phan,T.X., Yamakawa,H., Pao,P.C. *et al.* (2015) Activity-induced DNA breaks govern the expression of neuronal early-response genes. *Cell*, **161**, 1592–1605.
63. Szlachta,K., Manukyan,A., Raimer,H.M., Singh,S., Salamon,A., Guo,W., Lobachev,K.S. and Wang,Y.H. (2020) Topoisomerase II contributes to DNA secondary structure-mediated double-stranded breaks. *Nucleic Acids Res.*, **48**, 6654–6671.
64. Schellenberg,M.J., Lieberman,J.A., Herrero-Ruiz,A., Butler,L.R., Williams,J.G., Muñoz-Cabello,A.M., Mueller,G.A., London,R.E., Cortés-Ledesma,F. and Williams,R.S. (2017) ZATT (ZNF451)-mediated resolution of topoisomerase 2 DNA-protein cross-links. *Science*, **357**, 1412–1416.
65. Canela,A., Maman,Y., Huang,S.N., Wutz,G., Tang,W., Zagnoli-Vieira,G., Callen,E., Wong,N., Day,A., Peters,J.M. *et al.* (2019) Topoisomerase II-induced chromosome breakage and translocation is determined by chromosome architecture and transcriptional activity. *Mol. Cell*, **75**, 252–266.
66. Baranello,L., Wojtowicz,D., Cui,K., Devaiah,BallachandaN., Chung,H.-J., Chan-Salis,KaY., Guha,R., Wilson,K., Zhang,X., Zhang,H *et al.* (2016) RNA polymerase II regulates topoisomerase 1 activity to favor efficient transcription. *Cell*, **165**, 357–371.
67. Singh,S., Szlachta,K., Manukyan,A., Raimer,H.M., Dinda,M., Bekiranov,S. and Wang,Y.-H. (2020) Pausing sites of RNA polymerase II on actively transcribed genes are enriched in DNA double-stranded breaks. *J. Biol. Chem.*, **295**, 3990–4000.
68. Boyer,N.P., McCormick,L.E., Menon,S., Urbina,F.L. and Gupton,S.L. (2020) A pair of E3 ubiquitin ligases compete to regulate filopodial dynamics and axon guidance. *J. Cell Biol.*, **219**, e201902088.
69. Nicklas,S., Hillje,A.L., Okawa,S., Rudolph,I.M., Collmann,F.M., van Wuellen,T., Del Sol,A. and Schwamborn,J.C. (2019) A complex of the ubiquitin ligase TRIM32 and the deubiquitinase USP7 balances the level of c-Myc ubiquitination and thereby determines neural stem cell fate specification. *Cell Death Differ.*, **26**, 728–740.
70. Bonacci,T. and Emanuele,M.J. (2020) Dissenting degradation: deubiquitinases in cell cycle and cancer. *Semin. Cancer Biol.*, **67**, 145–158.
71. Kobayashi,T., Iwamoto,Y., Takashima,K., Isomura,A., Kosodo,Y., Kawakami,K., Nishioka,T., Kaibuchi,K. and Kageyama,R. (2015) Deubiquitinating enzymes regulate hes1 stability and neuronal differentiation. *FEBS J.*, **282**, 2411–2423.
72. Boyer,L.A., Lee,T.I., Cole,M.F., Johnstone,S.E., Levine,S.S., Zucker,J.P., Guenther,M.G., Kumar,R.M., Murray,H.L., Jenner,R.G. *et al.* (2005) Core transcriptional regulatory circuitry in human embryonic stem cells. *Cell*, **122**, 947–956.
73. Olivieri,M., Cho,T., Alvarez-Quilon,A., Li,K., Schellenberg,M.J., Zimmermann,M., Hustedt,N., Rossi,S.E., Adam,S., Melo,H. *et al.* (2020) A genetic map of the response to DNA damage in human cells. *Cell*, **182**, 481–496.
74. Qin,T., Li,B., Feng,X., Fan,S., Liu,L., Liu,D., Mao,J., Lu,Y., Yang,J., Yu,X. *et al.* (2018) Abnormally elevated USP37 expression in breast cancer stem cells regulates stemness, epithelial–mesenchymal transition and cisplatin sensitivity. *J. Exp. Clin. Cancer Res.*, **37**, 287.
75. Pan,J., Deng,Q., Jiang,C., Wang,X., Niu,T., Li,H., Chen,T., Jin,J., Pan,W., Cai,X. *et al.* (2015) USP37 directly deubiquitinates and stabilizes c-Myc in lung cancer. *Oncogene*, **34**, 3957–3967.
76. Andreu-Agullo,C., Maurin,T., Thompson,C.B. and Lai,E.C. (2011) Ars2 maintains neural stem-cell identity through direct transcriptional activation of sox2. *Nature*, **481**, 195–198.
77. Toda,T., Hsu,J.Y., Linker,S.B., Hu,L., Schafer,S.T., Mertens,J., Jacinto,F.V., Hetzer,M.W. and Gage,F.H. (2017) Nup153 interacts with sox2 to enable bimodal gene regulation and maintenance of neural progenitor cells. *Cell Stem Cell*, **21**, 618–634.